Since January 2020 Elsevier has created a COVID-19 resource centre with free information in English and Mandarin on the novel coronavirus COVID-19. The COVID-19 resource centre is hosted on Elsevier Connect, the company's public news and information website.

Cell

Imprinted SARS-CoV-2-specific memory lymphocytes define hybrid immunity

Graphical abstract

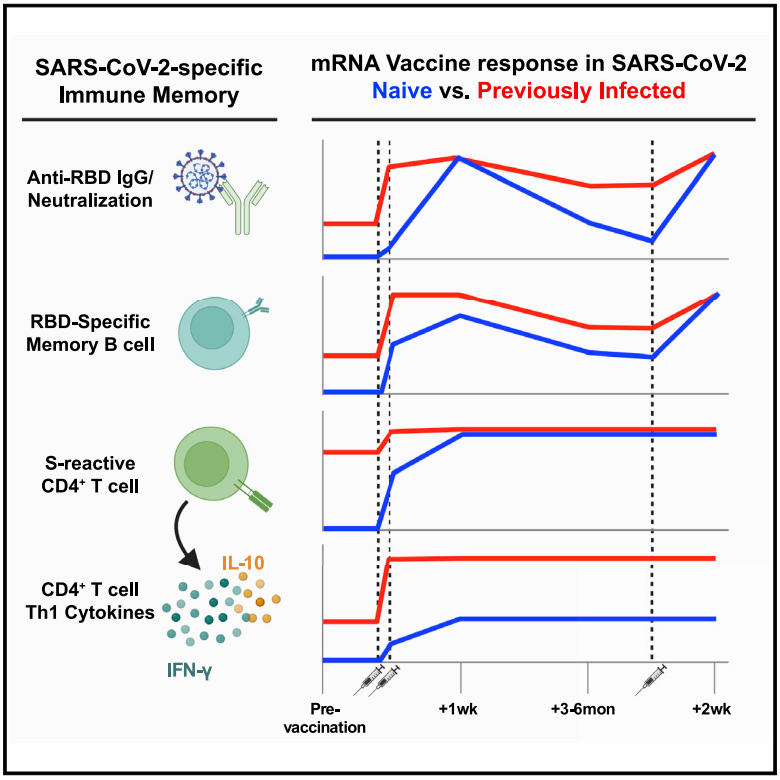

Authors

Lauren B. Rodda, Peter A. Morawski, Kurt B. Pruner, ..., Helen Y. Chu, Daniel J. Campbell, Marion Pepper

Correspondence

mpepper@uw.edu

In brief

The strong immunity against SARS-CoV-2 in vaccinated individuals that have previously been infected can be explained by a combination of RBD-specific memory B cells, variant-neutralizing antibodies, and a specific population of CD4$^+$ T cells.

Highlights

- Vaccination elicits robust SARS-CoV-2-specific immune memory regardless of prior infection
- Hybrid immunity is associated with more virus-specific memory B cells and Omicron nAb
- SARS-CoV-2 infection prior to vaccination elicits a robust CD4$^+$ T Th1/IFN-ɣ response
- Infection-induced Th1/IFN-ɣ signature is not reproduced by three vaccinations

Rodda et al., 2022, Cell *185*, 1588–1601
April 28, 2022
https://doi.org/10.1016/j.cell.2022.03.018

CellPress

CellPress

Cell

Article

Imprinted SARS-CoV-2-specific memory lymphocytes define hybrid immunity

Lauren B. Rodda,[1,6] Peter A. Morawski,[2,6] Kurt B. Pruner,[1,6] Mitchell L. Fahning,[2] Christian A. Howard,[1] Nicholas Franko,[3] Jennifer Logue,[3] Julie Eggenberger,[4] Caleb Stokes,[4] Inah Golez,[4] Malika Hale,[5] Michael Gale, Jr.,[4] Helen Y. Chu,[3] Daniel J. Campbell,[1,2] and Marion Pepper[1,7,*]

[1]Department of Immunology, University of Washington School of Medicine, Seattle, WA 98109, USA
[2]Center for Fundamental Immunology, Benaroya Research Institute, Seattle, WA 98101, USA
[3]Division of Allergy and Infectious Diseases, Department of Medicine, University of Washington, Seattle, WA 98109, USA
[4]Department of Immunology, Center for Innate Immunity and Immune Disease, University of Washington, Seattle, WA 98109, USA
[5]Center for Immunity and Immunotherapies, Seattle Children's Research Institute, Seattle, WA 98101, USA
[6]These authors contributed equally
[7]Lead contact
*Correspondence: mpepper@uw.edu
https://doi.org/10.1016/j.cell.2022.03.018

SUMMARY

Immune memory is tailored by cues that lymphocytes perceive during priming. The severe acute respiratory syndrome coronavirus 2 (SARS-CoV-2) pandemic created a situation in which nascent memory could be tracked through additional antigen exposures. Both SARS-CoV-2 infection and vaccination induce multifaceted, functional immune memory, but together, they engender improved protection from disease, termed hybrid immunity. We therefore investigated how vaccine-induced memory is shaped by previous infection. We found that following vaccination, previously infected individuals generated more SARS-CoV-2 RBD-specific memory B cells and variant-neutralizing antibodies and a distinct population of IFN-γ and IL-10-expressing memory SARS-CoV-2 spike-specific CD4$^+$ T cells than previously naive individuals. Although additional vaccination could increase humoral memory in previously naive individuals, it did not recapitulate the distinct CD4$^+$ T cell cytokine profile observed in previously infected subjects. Thus, imprinted features of SARS-CoV-2-specific memory lymphocytes define hybrid immunity.

INTRODUCTION

The generation of immune memory is influenced by signals that B and T lymphocytes of the adaptive immune system perceive during a primary immune response. This system has evolved such that key cues from an invading pathogen or vaccine are relayed to lymphocytes so that they can provide specific functional outputs to combat infection and protect from re-infection. The site of antigen encounter, specific inflammatory signals, and the number, timing, and frequency of antigen exposures all influence the resulting memory pool, yet the specific rules governing memory formation remain undefined. Understanding how the confluence of these parameters influences immune memory function and maintenance is critical for optimizing protective vaccines.

In the context of the ongoing severe acute respiratory syndrome coronavirus 2 (SARS-CoV-2) pandemic, the so-called "hybrid immunity" induced by a combination of prior SARS-CoV-2 infection and subsequent COVID-19 vaccination provides greater protection against re-infection and severe COVID-19 disease than either infection or vaccination alone (Abu-Raddad et al., 2021; Crotty, 2021; Gazit et al., 2021; Goldberg et al., 2021; Reynolds et al., 2021). Studies investigating immune correlates of hybrid immunity have revealed improved breadth and neutralizing ability of circulating antibodies from previously infected (PI) individuals (Cho et al., 2021; Schmidt et al., 2021b; Stamatatos et al., 2021; Wang et al., 2021), but the specific changes in the cellular immune compartment associated with this immune state remain undefined. Additionally, it is not understood whether further activation of immune memory in vaccinated-only individuals could achieve similar qualities, as PI individuals have had an additional antigen exposure.

To answer these questions, we tracked circulating SARS-CoV-2-specific antibodies and memory lymphocytes in a cohort of naive (N) or SARS-CoV-2-PI subjects over the course of three vaccinations. We focused on visualizing receptor binding domain (RBD)-specific antibodies and B cells, and spike (S)-specific CD4$^+$ T cells, as they are critical mediators of protection in infected individuals over a 2-year time period and induced by SARS-CoV-2-directed vaccines (Corbett et al., 2021; Feng et al., 2021; Gilbert et al., 2022; Khoury et al., 2021).

We find that the immune memory landscape elicited by vaccination of PI subjects is distinct from the immune memory of SARS-CoV-2-naive individuals. 3 months after two doses of

vaccination, PI individuals maintained a higher quantity of RBD-specific plasma antibodies with superior plasma neutralization of viral variants, including Omicron. PI individuals also retained increased numbers of RBD-specific B cells enriched for IgG^+ classical and activated memory B cells (MBCs) compared with N individuals. However, these differences were normalized by administration of a third vaccine dose. Examination of the T cell compartment revealed that although N and PI individuals generated equivalent numbers of S-specific $CD4^+$ T cells after vaccination, there was a profound functional skewing toward a Th1 phenotype in PI subjects. $CD4^+$ T cell functional differences between N and PI subjects persisted following the administration of a vaccine booster. Further, although the third dose of vaccine provided a boost in circulating antibodies, we observed no increase in memory T or B cells, indicating that the immune memory compartment is likely maximized after the two-dose regimen. Thus, our data support a model in which the priming environment induced by SARS-CoV-2 infection imprints immune memory with multiple features of enhanced type-1 antiviral immunity. These likely contribute to the increased protection associated with hybrid immunity and are not fully recapitulated by repeat vaccination.

RESULTS

The greater humoral response to vaccination in SARS-CoV-2 PI compared with N individuals is recovered by third vaccination

To investigate how prior SARS-CoV-2 infection impacts the quantity and quality of vaccine-induced SARS-CoV-2-specific immune memory, we collected plasma and peripheral blood mononuclear cells (PBMCs) from 24 SARS-CoV-2 N and 30 SARS-CoV-2 PI individuals before vaccination and 1 week, 3 months, and 6 months after two vaccinations with BNT162b2 (Pfizer-BioNTech) or mRNA-1273 (Moderna) COVID-19 vaccines (Figure 1A; Table 1; Baden et al., 2020; Polack et al., 2020). An average of 8 months following initial vaccination, 10 participants from each group received a third vaccine dose and we collected samples 2 weeks (mean: 18 days, SD: 8 days) later. N participants had no detectable SARS-CoV-2 RBD-specific IgG plasma antibodies above a cutoff set by historical negative (HN) controls prior to vaccination (Figure S1A). PI participants reported a positive SARS-CoV-2 test and mildly symptomatic disease an average of 9 months before their pre-vaccination blood draw.

To determine the distinct humoral features of hybrid immunity, we first compared the circulating SARS-CoV-2 RBD-specific B cells in N and PI participants pre and post-vaccination. Tetramer enrichment allowed us to identify rare SARS-CoV-2 RBD-specific B cells from PBMCs to track the memory response (Figure S1B). Pre-vaccination, PI individuals had significantly more RBD-specific antigen-experienced B cells ($CD21^+CD27^+$ and $CD21^-CD27^{+/-}$) (Cancro and Tomayko, 2021; Figures 1B, 1C, and S1C) and plasma RBD-specific IgG and IgA than N individuals (Figures 1D and 1E), reflecting the sustained memory response to their previous SARS-CoV-2 infection (Rodda et al., 2021; Dan et al., 2021). Two-dose vaccination induced a robust humoral response in both N and PI individuals, including increased numbers of RBD-specific antigen-experienced B cells (Figure 1C), an acute burst of RBD-specific plasmablasts (PBs) (Figure S1D), and increased titers of RBD-specific IgG and IgA antibody (Figures 1D and 1E). The numbers of RBD-specific antigen-experienced B cells and RBD-specific antibodies in both groups contracted to levels higher than those at pre-vaccination. However, PI individuals formed and retained higher numbers of RBD-specific antigen-experienced B cells and elevated RBD-specific IgG and IgA compared with N individuals at 3 and 6 months post-vaccination (Figures 1C–1E). These findings corroborate recent work and support the likely functional role of the elevated RBD-specific antibody and MBCs in hybrid immunity (Goel et al., 2021).

To determine if a third vaccine dose could overcome these differences by engaging the MBCs in N individuals in additional expansion, we measured the humoral response in both groups 2 weeks after a third dose. Although RBD-specific B cells in N individuals responded by increasing RBD-specific IgG and IgA antibody to the levels in PI individuals, the antibody response in N individuals to a third SARS-CoV-2 antigen exposure did not match the acute response in PI individuals to their third exposure (vaccination 2) (Figures 1D and 1E). This muted response to a third exposure in N and PI individuals may reflect efficient clearance of antigen by the high quantity of antigen-specific memory now established in both groups, and the increase in RBD-specific antibody in both groups is likely driven largely by short-lived PBs at 2 weeks post-third vaccination. Comparison of N and PI subjects several months post-third vaccination is required to determine if a third vaccination dose induces sustained expansion of RBD-specific MBCs and circulating antibody titers in N individuals that more closely match those in PI subjects.

Vaccination induces a robust and durable virus-specific $CD4^+$ T cell response irrespective of prior SARS-CoV-2 infection

$CD4^+$ T cell responses to vaccination were also assessed in N and PI individuals using an activation-induced marker (AIM) assay based on expression of CD69 and CD137 to detect SARS-CoV-2 specificity (Tarke et al., 2021; Figures S2A–S2F). PBMCs from N or PI participants isolated before and after vaccination were stimulated with SARS-CoV-2 spike (S) peptide pools optimized for the induction of MHC class II-dependent $CD4^+$ T cell responses (15-mers) and containing T cell epitopes across a range of common HLA haplotypes against the viral membrane and nucleocapsid (M/N) or S proteins (Data S1).

Pre-vaccination, $CD4^+$ T cells from PI participants showed responses to both M/N and S, consistent with prior SARS-CoV-2 infection and the presence of memory cells (Figures 2A and 2B), whereas responses in N participants were undetectable above individual donor background (Figures S2G and S2H). Throughout the course of vaccination, responses to M/N remained negative in N participants, but endured, undiminished in PI participants at all time points, indicating that SARS-CoV-2-specific $CD4^+$ T cells primed during infection, persist at least 18 months following initial antigen exposure (Figure 2B). Following initial two-dose vaccination, S-reactive AIM^+ $CD4^+$ T cells were significantly elevated above pre-vaccination levels in both N and PI individuals, with no significant differences in peak $CD4^+$ T cell response between groups (Figures 2B, S2G,

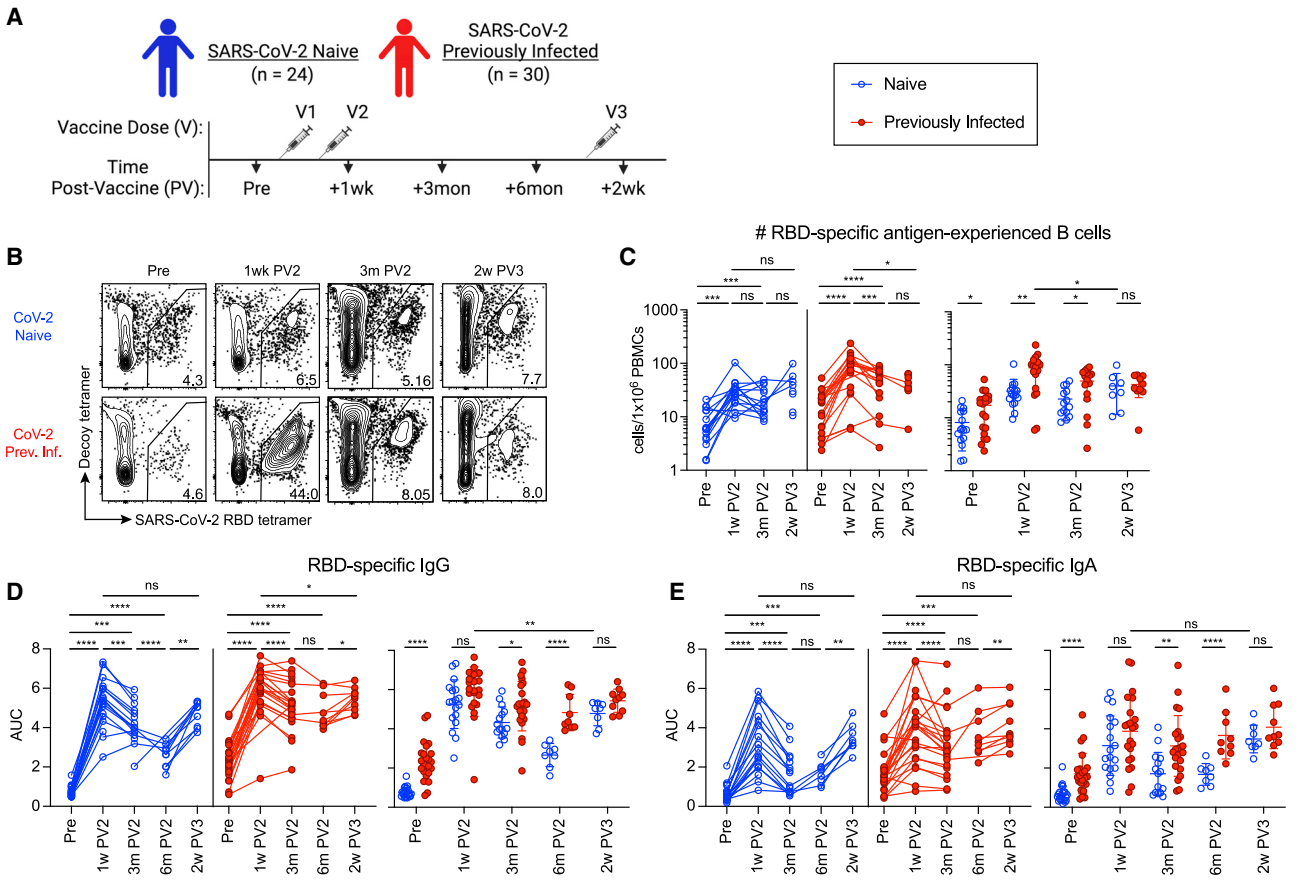

Figure 1. The greater humoral response to vaccination in SARS-CoV-2 previously infected compared with naive individuals is recovered by third vaccination

(A) Timeline of blood draws from SARS-CoV-2 naive (N) and previously infected (Prev. Inf., PI) analyzed in this study relative to vaccinations.

(B) Representative gating on CD19$^+$CD38^{lo} B cells for RBD-tetramer$^+$Decoy$^-$ SARS-CoV-2 RBD-specific B cells from N and PI (Prev. Inf.) PBMCs at the indicated time points pre-vaccination (Pre), 1 week post-second vaccination (1w PV2), 3 months post-second vaccination (3m PV2), and 6 months post-second vaccination (6m PV2).

(C) Number of RBD-specific antigen experienced (ag-exp.) B cells (CD21$^+$CD27$^+$ and CD21$^-$CD27$^{+/-}$) in N (blue) and PI (red) PBMCs at the indicated time points.

(D and E) ELISA area under the curve (AUC) for RBD-specific IgG (D) and IgA (E) plasma antibody from N and PI individuals at indicated time points.

Data in (C–E) are represented both longitudinally (left) and by cross-group comparisons (right). Statistics determined by Wilcoxon matched-paired signed rank test for longitudinal analyses and multiple unpaired Mann-Whitney test for group analyses: not significant (ns), *p < 0.05, **p < 0.005, ***p < 0.0005, and ****p < 0.0001. Error bars represent mean and SD.

See also Figure S1.

and S2H). Therefore, COVID-19 vaccination induces numerically equivalent populations of S-specific cells in all subjects, regardless of prior SARS-CoV-2 exposure status, which persist for at least 3 months.

We next examined the relative composition of effector and memory populations, including circulating T follicular helper (Tfh)-like cells (Ueno, 2016), within the SARS-CoV-2-reactive T cell compartment in N and PI subjects. Prior to vaccination, there was no difference in the frequency of S-reactive central memory (CM) T cells between N and PI groups; however, PI individuals maintained significantly elevated frequencies of CCR7$^-$CD45RA$^-$ effector memory (EM), CCR7$^-$CD45RA$^+$ effector memory (EMRA), and circulating Tfh cells (Figures 2C and 2D). Two-dose vaccination induced a significant increase in nearly all AIM$^+$ effector and memory populations in both groups, with EM and Tfh populations dominating the response (Figure 2D). In addition, two-dose vaccination was sufficient to normalize numerical differences identified in pre-vaccination N and PI participants, whereas a third dose was not associated with any additional increase in these populations in either N or PI participants (Figure 2D). Therefore, vaccination induces numerically equivalent S-specific memory Tfh and EM CD4$^+$ T cell responses in N and PI individuals that do not further increase in response to an additional vaccine dose.

Infection prior to vaccination corresponds with a sustained CD21$^-$CD11c$^+$-activated B cell response and superior SARS-CoV-2 variant-neutralizing antibody

MBCs function by activating, proliferating, and forming antibody-secreting PBs more rapidly than naive B cells (Cancro

Table 1. Study cohort characteristics

	SARS-CoV-2 naive	SARS-CoV-2 previously infected
Number of participants	24	30
Age (years)	46 (±16)[a]	50 (±17)
Sex	67% female, 33% male	77% female, 23% male
Sustained symptoms (PASC)[b]	N/A	10
Symptom onset to pre-vaccination draw (days)	N/A	265 (±89)
Symptom onset to vaccine dose 1 (days)	N/A	310 (±87)
Vaccine type[c]	9 mRNA-1273, 15 BNT162b2	10 mRNA-1273, 20 BNT162b2
Vaccine dose 2 to 1 week PV2[d] draw (days)	9 (±2)	10 (±4)
Vaccine dose 2 to 3 months PV2 draw (days)	93 (±11)	91 (±14)
Vaccine dose 2 to 6 months PV2 draw (days)	167 (±20)	160 (±16)
Participants that received vaccine dose 3	10	10
Vaccine dose 2 to vaccine dose 3	243 (±44)	233 (±24)
Vaccine dose 3 to 2 weeks PV3 draw (days)	20 (±10)	15 (±4)

[a]Mean (standard deviation).
[b]Participants surveyed at 6 months post-symptom onset for ongoing symptoms or post-acute sequelae of COVID-19 (PASC).
[c]mRNA-1273 (Moderna) or BNT162b2 (Pfizer-BioNTech).
[d]Post-vaccination 2 (PV2).

and Tamayko, 2021). Prior to vaccination, RBD-specific B cells in N individuals were predominantly naive ($CD21^+CD27^-$), whereas RBD-specific B cells in PI individuals were predominantly non-naive antigen-experienced B cells ($CD21^+CD27^+$ and $CD21^-CD27^{+/-}$) (Figures S3A and S3B). Two vaccinations induced an increase in the proportion and number of $CD21^-CD27^{+/-}CD11c^+$ B cells (Cancro and Tomayko, 2021) in both groups at 1 week post-vaccination with PI individuals displaying higher numbers than N individuals (Figures 3A and 3B). Although $CD21^-CD27^-CD11c^+$ "atypical MBCs" have been associated with chronic infection and autoimmunity, the expression pattern of these markers is also associated with recently activated B cells following acute antigen re-exposure. Although the proportion of $CD21^-CD11c^+$ activated MBCs decreased in both groups at 3 months post-infection, PI individuals retained higher numbers and a higher proportion than N individuals (Figure 3B). This may reflect prolonged antigen retention and a longer or larger ongoing germinal center (GC) response, which would contribute to the increased quantity of RBD-specific antigen-experienced cells, including classical MBCs and long lived plasma cells producing RBD-specific antibodies in PI individuals with hybrid immunity (Knox et al., 2017; Kim et al., 2019).

PI individuals also displayed higher proportions and numbers of IgG^+ classical MBCs (cMBCs, $CD21^+CD27^+$) among RBD-specific antigen-experienced cells compared with N donors prior to vaccination, indicative of their previous SARS-CoV-2 infection (Figure 3C). IgG^+ cMBCs rapidly form IgG-secreting PBs upon antigen exposure and are likely important to protection (Laidlaw and Ellebedy, 2022). Due to the expansion of $CD21^-CD11c^+$-activated MBCs, IgG^+ cMBCs made up a reduced proportion of the RBD-specific antigen-experienced cells in both groups at 1 week post-vaccination. In response to vaccination, the numbers of IgG^+ cMBCs increased in both groups at 1 week post-vaccination. The numbers of IgG^+ cMBCs in N individuals further increased at 3 months post-vaccination but did not quite reach the numbers of IgG^+ cMBCs in PI subjects at this time point. N and PI individuals presented similar frequencies of IgG^+ cMBCs at 3 months post-vaccination. This quantitative gap between N and PI individuals was subsequently normalized by a third dose of vaccine (Figure 3C). Thus, the higher number of IgG^+ cMBCs in PI individuals likely contributes to immune protection associated with hybrid immunity and this benefit can also be achieved by three vaccinations. Although mucosal infections such as SARS-CoV-2 are associated with IgA^+ MBCs, particularly at the site of infection, PI individuals had only a small proportion of circulating IgA^+ RBD-specific antigen-experienced B cells at 9 months post-infection, and they were not further induced in N or PI individuals by vaccination (Figure S3C).

To assess if infection prior to vaccination impacts the breadth or ability of SARS-CoV-2-specific MBCs and antibodies to recognize and combat SARS-CoV-2 variants of concern (VOCs), we measured the ability of RBD-specific MBCs and antibody to recognize the B.1.351 (Beta, β) variant and plasma antibody to neutralize the B.1.617.2 (Delta, Δ) and B.1.1.529 (Omicron, o) variants. SARS-CoV-2(β) and SARS-CoV-2(o) have been found to significantly reduce neutralization by vaccine-induced antibodies as compared with the original SARS-CoV-2(Wu-1) strain, which was also used to make the mRNA vaccines relevant to this study (Cameroni et al., 2021; Collier et al., 2021). Using SARS-CoV-2 RBD(Wu-1) and SARS-CoV-2 RBD(β) tetramers simultaneously (Figure S1B), we found that the majority of RBD-specific antigen-experienced B cells in all N and PI participants could recognize both variants (Figures S3D and S3E). This technique does not allow us to distinguish cross-reactive cells that bind epitopes shared by the variant RBDs from cells that bind epitopes with the three amino acid differences between the variants. Although vaccination induced increased RBD(β)-specific IgG antibody titers in both groups, PI individuals had significantly higher RBD(β)-specific IgG titers than N individuals pre- and 6 months post-vaccination (Figure S3F). This is corroborated by similar

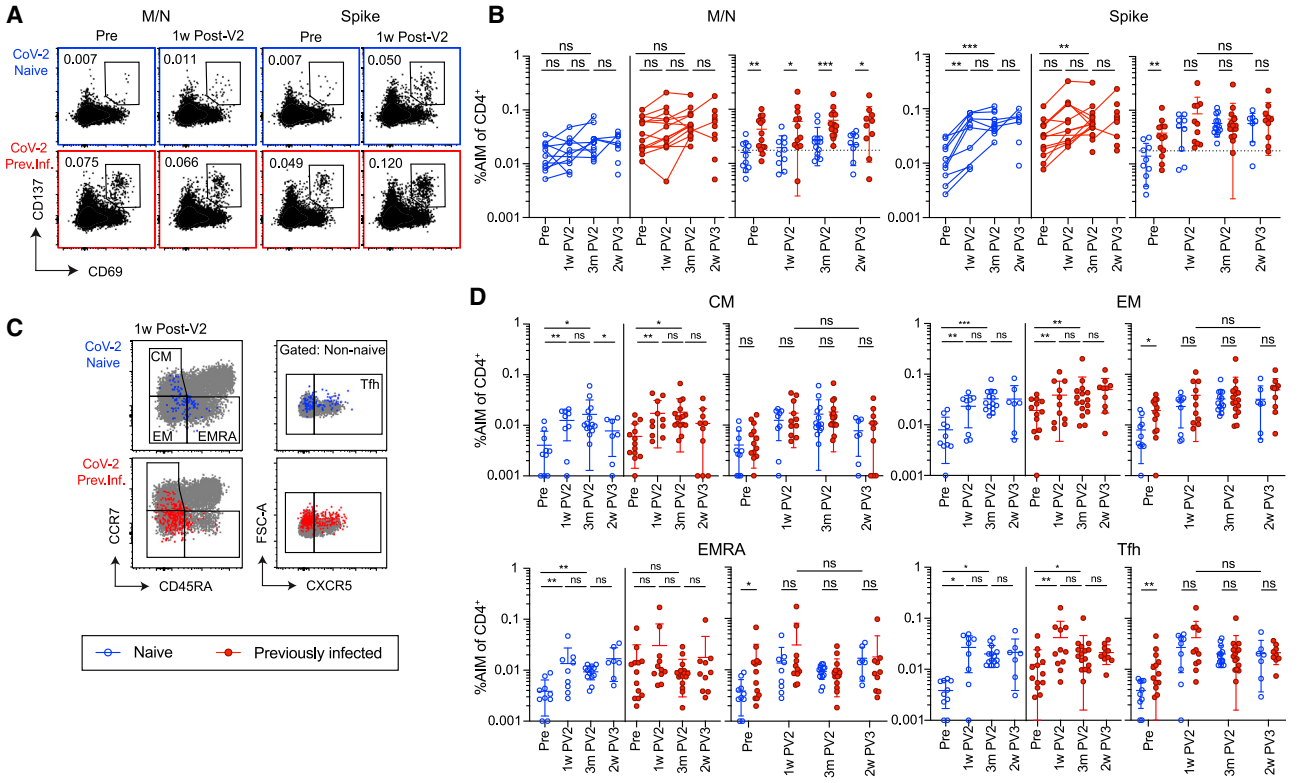

Figure 2. Robust and durable CD4⁺ T cell responses to SARS-CoV-2 in both previously naive and previously infected individuals

Analysis of non-naive CD4⁺CD69⁺CD137⁺ T cells (AIM CD4⁺) in SARS-CoV-2 naive (blue) and previously infected (red) individuals.

(A and B) Representative flow cytometry plots and summary graphs for total AIM CD4⁺ T cells. T cell responses shown are either to SARS-CoV-2 membrane and nucleocapsid (M/N) or spike peptide pools for each donor.

(C and D) Representative flow cytometry plots and summary graphs of indicated AIM CD4⁺ memory and Tfh subsets for participants shown in (A) and (B). Data in (B) and (D) are represented both longitudinally (left) and by cross-group comparisons (right).

Significance was determined by Wilcoxon matched-paired signed rank test for longitudinal analyses and multiple unpaired Mann-Whitney test for group analyses: not significant (ns), *p < 0.05, **p < 0.01, ***p < 0.001, and ****p < 0.0001. Error bars represent mean and SD. Dashed lines indicate average donor background level. Central memory (CM), effector memory (EM), T effector memory CD45RA⁺ (TEMRA), T follicular helper (Tfh). Pre-vaccination (Pre), 1 week post two-dose COVID-19 mRNA vaccination (1w PV2), 3 months post two-dose vaccination (3m PV2), 2 weeks post third vaccination dose (2w PV3). See also Figure S2 and Data S1.

recent findings (Stamatatos et al., 2021). Additionally, we found that plasma from PI individuals 6 months post-vaccination was significantly better at neutralizing SARS-CoV-2(WA-1) virus (Figures 3D and S3G), as well as pseudotyped SARS-CoV-2(Δ)-spike and SARS-CoV-2(o)-spike lentiviruses than plasma from N individuals (Figures 3E and S3G). SARS-CoV-2(WA-1) neutralization was highly correlated with RBD(Wu-1)-specific IgG antibody titers as we and others have shown previously, and the higher titers in PI individuals post-vaccination likely contribute to the improved variant neutralization over N individuals (Figure S3H; Rodda et al., 2021; Goel et al., 2021). The increased antibody response to a third vaccine dose in N individuals (Figures 1D, 1E, and S3F) correlated with sharply increased neutralization capacity of the plasma antibody against the variants tested reaching the levels in PI individuals pre- and post-third vaccination (Figures 3D and S3F). Thus, vaccination induces robust humoral memory in N and PI participants, but a third dose is needed for N individuals to achieve the breadth and VOC neutralizing activity of the plasma antibody formed in hybrid immunity.

Infection induces functionally distinct SARS-CoV-2-specific CD4⁺ T cell responses that are not attributed solely to the number of antigen exposures

During T cell priming, the context of the initial antigen exposure directs CD4⁺ T cells toward different helper and memory fates with distinct functional capacities. To determine how a primary infection versus vaccination or total number of antigen exposures differentially impacted functional outcomes, we compared the CD4⁺ T helper lineage composition of SARS-CoV-2 AIM⁺ T cells based on differential chemokine receptor expression in N and PI subjects. Prior to vaccination, we found that S-reactive T cells in PI subjects were primarily Th1 and Th1/17 memory cells (Figures 4A and 4B). In response to vaccination, S-reactive cells displayed features of activation, such as the downregulation of CD127 (Figure S4A), and the frequency of S-specific cells increased in nearly all T helper subsets examined in both N and PI individuals, consistent with previous reports (Goel et al., 2021; Guerrera et al., 2021; Painter et al., 2021). However, PI subjects maintained an elevated frequency of

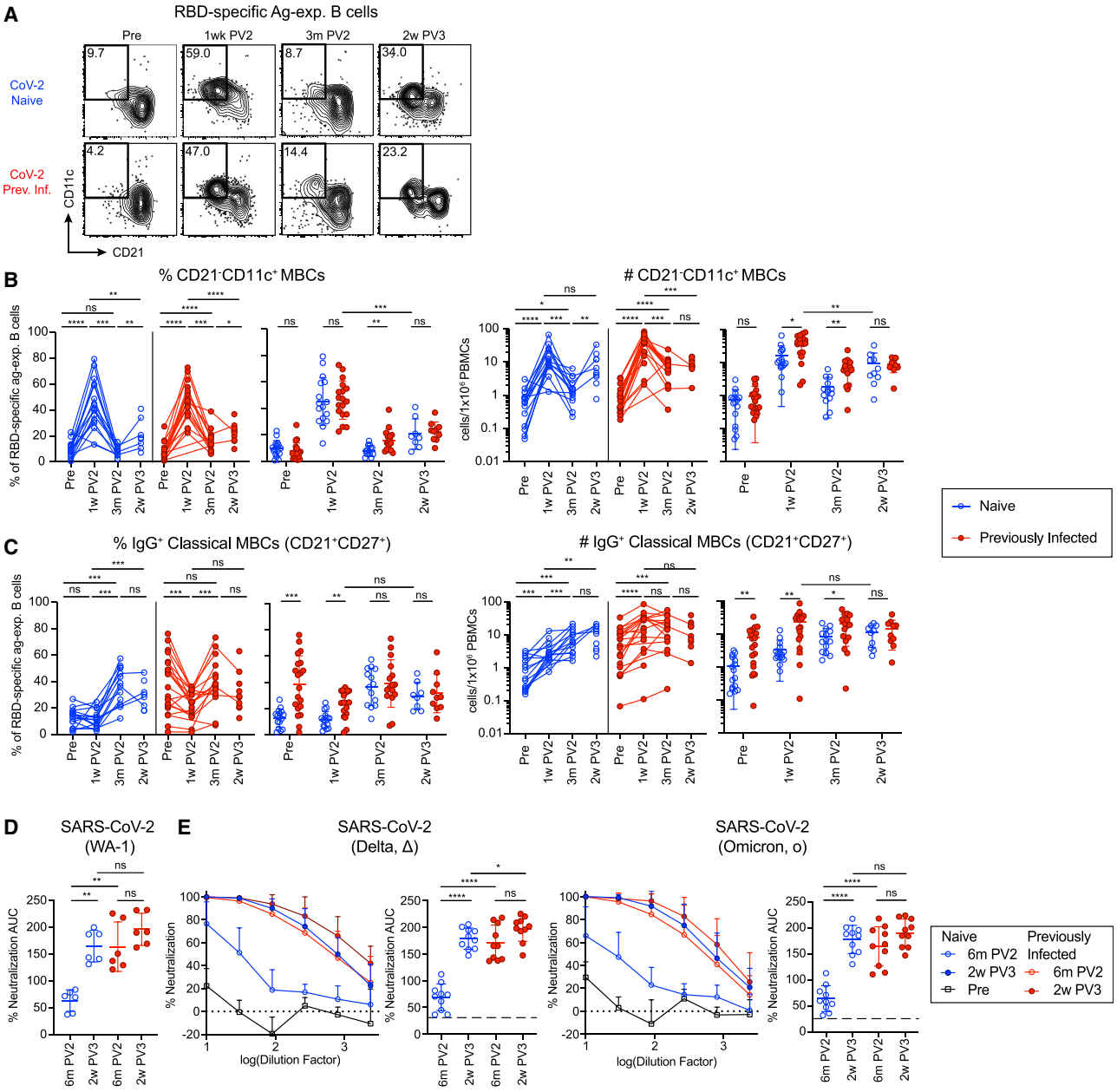

Figure 3. Infection prior to vaccination corresponds with sustained CD21$^-$CD11c$^+$ MBCs and superior SARS-CoV-2 variant-neutralizing antibody

(A) Representative gating on RBD-specific antigen-experienced (ag-exp.) B cells for activated MBCs (CD21$^-$CD11c$^+$) from N and PI PBMCs at the indicated time points.

(B and C) (B) Percent and number of activated MBCs and (C) percent and number of IgG$^+$ classical MBCs (CD21$^+$CD27$^+$) of RBD-specific ag-exp. B cells in N and PI PBMCs at the indicated time points.

(D) Percent neutralization AUC of SARS-CoV-2 (WA-1) by plasma from N and PI individuals at the indicated time points by PRNT.

(E) Percent neutralization of SARS-CoV-2(Delta, Δ) and SARS-CoV-2(Omicron, o) spike-pseudotyped virus by plasma from N and PI individuals at the indicated time points (left). Percent neutralization area under the curve (AUC) (right). Dashed line indicates the average percent neutralization of plasma from N individuals pre-vaccination. Data in (B) and (C) are represented both longitudinally (left) and by cross-group comparisons (right). Statistics determined by Wilcoxon matched-paired signed rank test for longitudinal analyses and multiple unpaired Mann-Whitney test for group analyses: not significant (ns), *p < 0.05, **p < 0.005, ***p < 0.0005, and ****p < 0.0001. Error bars represent mean and SD. Pre-vaccination (Pre), 1 week post two-dose COVID-19 mRNA vaccination (1w PV2), 3 months post two-dose vaccination (3m PV2), 2 weeks post third vaccination dose (2w PV3). See also Figure S3.

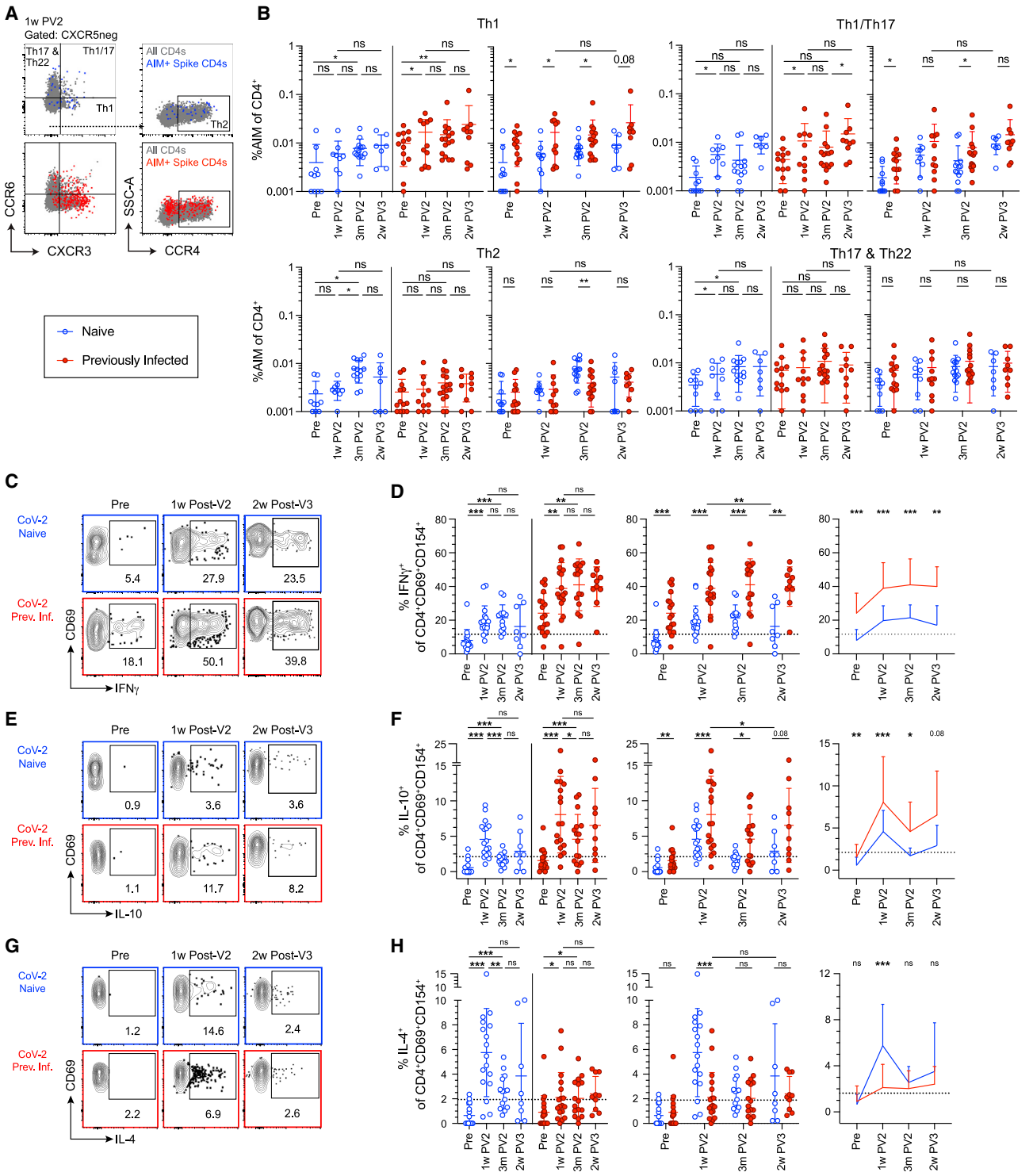

Figure 4. CD4⁺ T cell responses to SARS-CoV-2 demonstrate qualitative effector cell differences between previously naive and previously infected individuals

Analysis of spike-reactive CD4⁺ T cells in SARS-CoV-2 naive (blue) and previously infected (red) individuals.

(A and B) Representative flow cytometry plots, gating scheme, and summary graphs for non-naive CD4⁺CD69⁺CD137⁺ T cells (AIM CD4⁺) for the indicated T helper subsets.

(C–H) Representative flow cytometry plots and summary graphs for the indicated cytokines, gated on total CD4⁺CD69⁺CD154⁺ T cells.

(legend continued on next page)

both CXCR3$^+$CCR6$^-$ Th1 and CXCR3$^+$CCR6$^+$ Th1/17 cells, whereas N participants showed increased numbers of CXCR3$^-$CCR6$^-$CCR4$^+$ Th2 cells by 3 months post-vaccination 2 (Figure 4B). Th1 and Th1/17 AIM$^+$ cells continued to trend higher in PI individuals following a third vaccine dose, but this difference did not reach statistical significance. In addition, at this acute time point post-vaccination 3, the frequency of Th2 populations were normalized between groups (Figure 4B). These data demonstrate that T helper polarization in response to initial vaccination differs according to prior SARS-CoV-2 infection status and that additional vaccine doses may have a normalizing effect on some aspects of this response.

To complement the phenotypic analysis of CD4$^+$ T cells, we employed a similar assay to directly interrogate cytokine production from SARS-CoV-2-specific CD4$^+$ T cells following stimulation with M/N or S peptide pools. As demonstrated previously, CD154 and CD69 can be used to identify activated, antigen-reactive T cells (Reiss et al., 2017) that represent the primary cytokine producers in response to stimulation (Figures S4B and S4C). Importantly, the response measured in CD154$^+$CD69$^+$ SARS-CoV-2 reactive T cells to peptide stimulation mirrors that of AIM$^+$ CD69$^+$CD137$^+$ cells shown in Figure 2, including an M/N response exclusive to PI subjects and robust induction of S-specific cells following two-dose immunization that was maintained after a third vaccination dose in both groups (Figures S4D–S4F).

In PI subjects, we measured a strong cytokine response to infection in M/N- (Figures S5A–S5E) and S-reactive T cells (Figures 4C–4F, S6A, and S6B) that was dominated by the production of IFN-γ and IL-2 but also included modest levels of IL-10. Cytokine production in response to M/N peptides in PI individuals was not enhanced by vaccination (Figures S5A–S5E). Neither N nor PI donor S-reactive T cells produced any detectable IL-4 (Figures 4G and 4H), IL-21, IL-13, IL-17, CD107a, or IL-22 (Figures S6C–S6H) prior to vaccination. The response in N individuals to two doses of vaccination generated a functionally diverse CD4$^+$ T cell response, exhibiting strong induction of IFN-γ, IL-10, IL-4 (Figures 4C–4H), IL-2, and IL-21 (Figures S6A–S6D), whereas we observed no increased expression of IL-17A, CD107a, or IL-22 over pre-vaccination levels (Figures S6F–S6H). IL-4 production, a hallmark of both Th2 and Tfh CD4$^+$ T cell responses (Ruterbusch et al., 2020), was enriched specifically at 1 week post-vaccination in N individuals (Figures 4G and 4H). However, few spike-reactive T cells co-produced IL-4 and IL-13 (Figure S6E), suggesting the absence of bona fide Th2 polarization. Consistent with our phenotypic analysis of T helper polarization based on differential chemokine receptor expression, PI individuals not only exhibited a strong induction of IFN-γ-producing S-reactive CD4$^+$ T cells following vaccination, but also this response remained significantly elevated compared with the N group following both second and third vaccine doses (Figures 4C and 4D). PI donor CD4$^+$ T cells also produced higher levels of IL-10 after two-dose vaccination compared with N participants, which also trended higher after a third vaccine dose despite failing to reach statistical significance (Figures 4E and 4F). Production of IL-21, although not detected following infection, was observed at comparable levels in both N and PI individuals following two- and three-dose vaccination (Figures S6C and S6D).

The S-reactive CD4$^+$ T cell compartment was further distilled into subpopulations using a dimensionality reduction analysis on pooled CD154$^+$CD69$^+$ cells from all participants. We applied uniform manifold approximation and projection (UMAP) followed by FlowSOM analysis and identified 15 distinct clusters of which 13 were expanded following infection or vaccination, and six included cells that produced cytokine(s) (Figures 5A–5P). Two of these clusters, CL4 and CL13, were specifically enriched in PI donor T cells following vaccination. CL4 was defined largely by the production of IFN-γ and low CD127 expression, indicative of terminally differentiated Th1 cells (Figure 5E). CL13 was defined by co-production of IFN-γ and IL-10, while also displaying low CD127 expression, resembling FOXP3$^-$ type-1 regulatory (Tr1) cells (Figure 5N; Jankovic et al., 2007; Sun et al., 2009). In contrast, increased vaccine-induced T cells producing IL-4 were specifically enriched in CL15 only in N participants. These cells additionally co-produced IL-2, IFN-γ, and small amounts of IL-21 (Figure 5P), suggesting a Tfh-like phenotype (Olatunde et al., 2021). Collectively, this unbiased analysis of the S-reactive CD4$^+$ T cell compartment identifies the emergence of functionally distinct subsets, which differ following vaccination in PI and N participants according to prior SARS-CoV-2 infection history.

To determine how the number of antigen exposures may alter distinct cytokine production profiles seen in N and PI individuals, we compared S-reactive T cells from N individuals after three doses of vaccination (three antigen exposures) with those from PI individuals after two doses of vaccination (three antigen exposures). A comparison of AIM$^+$ S-specific CD4$^+$ T cells in triple-vaccinated N subjects with double-vaccinated PI individuals normalized differences between Th1 and Th1/17 frequencies as assessed by CXCR3 and CCR6 expression (Figures 4A and 4B). We also found similar frequencies of CM, EM, EMRA, and Tfh cells when normalizing for the number of antigen exposures (Figures 2B and 2D). However, when cytokine production was assessed between triple-vaccinated N participants and double-vaccinated PI participants, the PI group maintained a dramatically elevated frequency of IFN-γ- and IL-10-producing S-specific CD4$^+$ T cells compared with the N group (Figures 4C and 4D). These data indicate that T cell priming by infection or vaccination promotes distinct effector states in which phenotypic outcomes can be normalized by additional antigen exposure, whereas functional differences persist through multiple vaccine doses.

Data in (B), (D), (F), and (H) are represented both longitudinally (left) and by cross-group comparisons (middle, right). Significance was determined by Wilcoxon matched-paired signed rank test for longitudinal analyses and multiple unpaired Mann-Whitney test for group analyses: not significant (ns), *$p < 0.05$, **$p < 0.01$, ***$p < 0.001$, and ****$p < 0.0001$. Error bars represent mean and SD. Dashed lines indicate average donor background level. Pre-vaccination (Pre), 1 week post two-dose COVID-19 mRNA vaccination (1w PV2), 3 months post two-dose vaccination (3m PV2), 2 weeks post third vaccination dose (2w PV3).
See also Figures S4–S6.

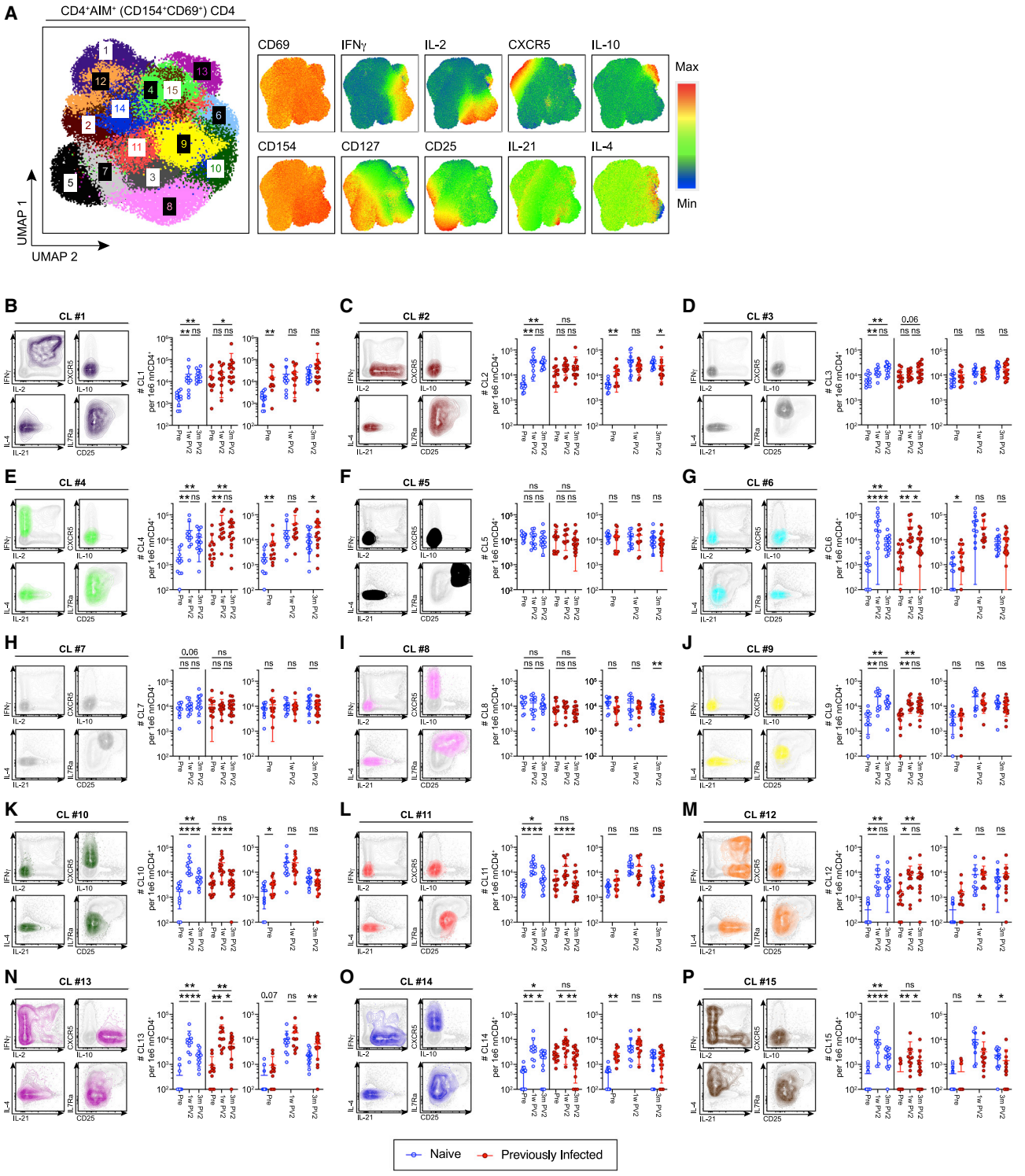

Figure 5. Dimensionality reduction and clustering analysis of SARS-CoV-2 S-specific CD4$^+$AIM$^+$ T cells

(A) Dimensionality reduction and phenograph-derived clustering (k = 40) overlaid for total CD4$^+$AIM$^+$(CD154$^+$CD69$^+$) T cells pooled from all participants (left). Heatmap expression of the indicated parameters over UMAP space (right).

(B–P) All cells from the indicated clusters (CL) are represented in corresponding color from UMAP plot in (A) overlayed on all CD4$^+$AIM$^+$ T cells and showing expression of select parameters (IL-2, IFN-γ, IL-10, CXCR5, CD127, CD25, IL-4, and IL-21). Enumeration of each cluster is per 1 × 10^6 non-naive (nn) CD4$^+$

(legend continued on next page)

DISCUSSION

Protective immunity generated in response to infection or vaccination is characterized by an expanded population of antigen-specific memory cells that rapidly expresses effector molecules upon antigen re-exposure. In order to prevent or control re-infection, memory cells are functionally tailored by the initial priming event; however, it is unclear how subsequent antigen exposures alter the quantity and quality of the response. The emergence of a novel coronavirus and expeditious generation of vaccines provided an unprecedented opportunity to examine the formation of a nascent antigen-specific memory pool in human volunteers and the impact of previous infection on the quantity, quality, and durability of vaccine-induced immune memory. This is particularly important, as SARS-CoV-2 infection prior to vaccination, referred to as "hybrid immunity," provides a protective advantage over vaccination alone (Abu-Raddad et al., 2021; Crotty, 2021; Gazit et al., 2021; Goldberg et al., 2021).

In this study, we examined the distinguishing features of hybrid immunity to SARS-CoV-2 in comparison with vaccination alone over time and with subsequent antigen exposures. We found that infection prior to vaccination induced higher numbers of RBD-specific MBC, more sustained IgG and IgA circulating antibodies, and increased plasma neutralization of multiple VOCs, including SARS-CoV-2 (Omicron). RBD-binding and neutralizing antibody has been proposed to be essential to the enhanced protection described in PI individuals after vaccination (PV2) (Cho et al., 2021; Schmidt et al., 2021a, 2021b; Stamatatos et al., 2021; Wang et al., 2021). These features were normalized following booster vaccination and therefore could be a function of the number of antigen exposures. However, although SARS-CoV-2 infection and COVID-19 immunization both induce robust Th1 immune memory, as found here and by other groups (Goel et al., 2021; Guerrera et al., 2021; Painter et al., 2021), we found that the spike-specific $CD4^+$ T cells induced in PI and then vaccinated individuals exhibited a unique IFN-γ and IL-10 cytokine-producing profile not recapitulated in N individuals by repeat vaccination. This represents the first immune correlate of hybrid immunity that is stably imprinted on responding cells during initial infection and could contribute to protection from symptomatic infection by providing an antiviral program.

There are many parameters that could contribute to the distinct, vaccine-induced immune responses seen in N or PI individuals, including the timing, route, or inflammatory conditions associated with a given SARS-CoV-2 antigen exposure. In this study, we were able to control for the number of antigen exposures by comparing double- and triple-vaccinated N and PI individuals. However, the timing of exposures varies substantially between the groups. In PI individuals, the first and second exposures to antigen were separated by ~10 months, whereas in N individuals, the time between first and second exposures was only ~3.5 weeks. Longer intervals between vaccinations in N individuals results in more neutralizing antibody and more SARS-CoV-2-specific B cells, which could then drive a larger response given a subsequent antigen exposure (Payne et al., 2021). The benefit of time was seen again in N individuals receiving their third vaccine 8 months after their second, which likely helped to normalize quantitative differences in SARS-CoV-2-specific antibody and MBCs seen in N and PI individuals post-vaccination 3.

We found that RBD-specific MBCs in PI individuals sustained a higher proportion and number of $CD21^-CD11c^+$-activated MBCs at 3 months post-vaccination 2 (after three exposures). Work by Pape et al. also found that after two exposures, PI individuals had higher numbers of $CD21^-CD27^-CD11c^+$ MBCs than N individuals (Pape et al., 2021), further suggesting that this could be an imprinted quality of prior infection or a difference in the quality of MBCs responding to vaccination as discussed above. $CD21^-CD11c^+$ memory cells have been described in the varied contexts of chronic viral infection, autoimmunity, and vaccination and found to have similarly varied features, including T-bet expression, potent antigen presentation, recent activation, and resistance to activation (Knox et al., 2017; Glass et al., 2020). The COVID-19 mRNA vaccines induce GC responses that last for months in N individuals, but whether they are larger or last longer in PI individuals is yet to be determined (Turner et al., 2021a, 2021b; Cho et al., 2021; Kim et al., 2021). We hypothesize that $CD21^-CD11c^+$ MBCs are likely recently activated and may be the result of ongoing GC responses and the sustained antigen driving them. This population could be larger in PI subjects because they are further supported by the elevated frequency of IFN-γ-expressing $CD4^+$ T cells, which can drive T-bet expression and support B cell activation. Larger and longer GCs support the generation of high affinity and broadly neutralizing antibodies, which are critical for combating variants and are likely contributing to the protective advantage of hybrid immunity (Turner et al., 2021b; Goel et al., 2021). Additional data from several months after a third vaccination are needed to determine whether this enhanced activation can be matched in N individuals by repeat vaccination.

Differences in route or inflammation associated with antigen exposure between N and PI individuals are likely key factors contributing to the differences in T cell phenotype and functionality associated with hybrid immunity. Pulmonary infection with SARS-CoV-2 virus and intramuscular immunization with full-length spike mRNA involve distinct inflammatory environments for immune activation to spike protein. Prolonged viral replication in pulmonary tissue has been associated with production of various inflammatory cytokines in COVID-19 patients (Galani et al., 2021; Lucas et al., 2020). Specifically, the inflammatory cytokines IL-12, IFN-α, and IFN-γ, produced by innate lymphocytes in response to viral PAMPs, directly drive T cells to upregulate the transcription factor T-bet, the master transcription factor for Th1 cells (Brinkmann et al., 1993; Lazarevic et al., 2013), and may induce the $CD4^+$ memory T cell IFN-γ and IL-10 signature we describe in PI individuals that is maintained through vaccination. Further, the cytokines IL-6, IL-12, or IL-27 drive the expression of IL-10 in $FOXP3^-$ $CD4^+$ helper T cells through the adapter

T cells in SARS-CoV-2 naive (blue) and SARS-CoV-2 previously infected (red) participants. Pre-vaccination (Pre), 1 week post two-dose COVID-19 mRNA vaccination (1w PV2), 3 months post two-dose vaccination (3m PV2). Significance was determined by multiple unpaired Mann-Whitney test for group analyses and by Wilcoxon matched-paired signed rank test for longitudinal analyses: not significant (ns), *$p < 0.05$, **$p < 0.01$.

c-maf (Gabryšová et al., 2018; Pot et al., 2009; Yang et al., 2005). Functional differences, including the production of IL-10, have previously been described in SARS-CoV-2-specific $CD4^+$ T cells from individuals that experienced different levels of COVID-19 severity, raising questions about how these cytokines may be involved in immune protection (Le Bert et al., 2021).

Additionally, infection with SARS-CoV-2 recruits effector T cells to the lung tissue, generating tissue-resident memory (Trm) cells in the human lung (Poon et al., 2021). T cells that enter the lung tissue or interact with lung-derived innate cells in the lung-draining lymph node, may encounter a distinct inflammatory environment not present during intramuscular mRNA vaccination. Indeed, tissue-experienced $CD4^+$ Trm cells produce the highest levels of IFN-γ and IL-10 in a mouse-adapted SARS-CoV infection (Zhao et al., 2016). Therefore, it may be the case that the increase in cytokine production we see in PI participants is due to the presence of circulating S-reactive T cells, which previously received tissue-specific cues. Although primarily studied in the mouse, Trm cells have been shown to be able to re-enter the circulating memory T cell compartment from the intestine in a phenomenon termed "retrograde migration" following systemic lymphocytic choriomeningitis virus (LCMV) or vesicular stomatitis virus (VSV) infections, as well as from the lung following influenza infection (Wijeyesinghe et al., 2021; Fonseca et al., 2020; Stolley et al., 2020). A similar phenomenon has also been described in humans, as skin-resident $CD4^+$ Trm cells can re-enter the blood (Klicznik et al., 2019). This raises the possibility that lung-transiting CoV-2-specific T cells may be captured in AIM assays of PBMCs and contribute to the increased cytokine production we observe in PI donors.

The distinct $CD4^+$ T cell cytokine signature we describe likely contributes to the increased protection observed in PI individuals with hybrid immunity. IFN-γ is produced rapidly by memory T cells *in vivo*, driving an antiviral response program, which is characterized by the upregulation of interferon-stimulated genes. Our data showing elevated frequencies of IFN-γ-producing memory $CD4^+$ T cells in PI individuals and the observed localization of $CD4^+$ Trm in the lung (Poon et al., 2021) together support a model in which early antiviral programs are bolstered rapidly by the inclusion of memory T cells locally at the site of infection. Indeed, pre-treatment of naive mice with recombinant IFN-γ completely inhibits SARS-CoV infection of the lung (Zhao et al., 2016). This study also reported that concomitant treatment with recombinant TNF-α exacerbates SARS-CoV-mediated disease in mice. IL-10 can inhibit TNF-α and other pro-inflammatory cytokines in order to regulate inflammatory responses to infection (O'Garra and Vieira, 2007; De Waal Malefyt et al., 1991; Gazzinelli et al., 1996; Hunter et al., 1997). Therefore, increased production of IL-10 by S-specific Th1 cells potentiated through viral infection could be a critical element of hybrid immunity that limits future symptomatic SARS-CoV-2 infection. Additional work is needed to explore this crucial role of memory T cell-derived IL-10 in secondary challenge.

The protective advantage of hybrid immunity likely stems from a combination of higher numbers of SARS-CoV-2-specific MBCs, higher neutralizing antibody titers, and the infection-imprinted IFN-γ and IL-10 cytokine profile in $CD4^+$ T cells. These features were not as highly induced in solely vaccinated individuals even with a third antigen exposure via vaccination. Future work is needed to determine how the relative timing of infection versus vaccination quantitatively and qualitatively impacts functional SARS-CoV-2 immune memory. The reduced immune response to the third vaccination in both groups as compared with the first two suggests that further homologous vaccinations are unlikely to bolster SARS-CoV-2 cellular immune memory. Therefore, as additional viral variants evolve to further evade immune memory, future vaccination strategies should focus on expanding the pool of SARS-CoV-2-specific memory cells and increasing the titers of viral variant-neutralizing antibodies. To do this, additional vaccine doses likely need to include variant spike proteins to engage a broader repertoire of immune cells and induce further cross-reactive memory responses.

Limitations of the study

First, we were not able to determine if a third vaccination induced better sustained RBD-specific antibodies or activated MBCs because we analyzed samples only 2 weeks after the third dose when short-lived PBs could be contributing to plasma antibody and MBCs are likely still expanding. Second, we studied immune memory only from peripheral blood, restricting our understanding of how prior infection impacts tissue-resident memory and the role it may play in hybrid immunity. Third, we identified spike-specific T cells by incubating with 15-mer peptide pools, which induced a robust response from MHC-II-restricted $CD4^+$ T cells but may not have been ideal for activating $CD8^+$ T cells, which recognize shorter peptides presented on MHC-I.

STAR★METHODS

Detailed methods are provided in the online version of this paper and include the following:

- KEY RESOURCES TABLE
- RESOURCE AVAILABILITY
  - Lead contact
  - Materials availability
  - Data and code availability
- EXPERIMENTAL MODEL AND SUBJECT DETAILS
  - Ethics statement
  - Human study participants and clinical data
  - Cell lines
- METHOD DETAILS
  - Sample processing and plasma collection
  - SARS-CoV-2 RBD protein and tetramer generation
  - Enzyme-linked immunosorbent assay (ELISA)
  - SARS-CoV-2 spike pseudotyped lentivirus
  - Pseudovirus neutralization test (pVNT)
  - Plaque reduction neutralization test (PRNT)
  - Peptide mesopools
  - Activation induced marker assay
  - Immunophenotyping of PBMCs
  - Fluorescence flow cytometry
  - High-dimensional analysis of cytometry data
- QUANTIFICATION AND STATISTICAL ANALYSIS
  - Statistics

SUPPLEMENTAL INFORMATION

Supplemental information can be found online at https://doi.org/10.1016/j.cell.2022.03.018.

ACKNOWLEDGMENTS

We thank the participants of the HAARVI Research study, Healthy Adult Specimen Repository study, and COVID-19/SARS-CoV-2 Prevalence and Antibody Therapy Development study; Megan Kemp and Jen Rathe for sample procurement; Kristin Huden and Callista Nackviseth for sample processing; Jason Netland and Laila Shehata for sample processing and technical help; Lauren Carter (Neil P. King lab) and John Bowen (David Veesler lab) for RBD(Wu-1) and RBD(β) protein; Adam Wojno and the BRI Cell and Tissue Imaging Core and U. Washington Cell Analysis Facility for technical help; Wesley C. Van Voorhis for HN plasma samples; Hannah Deberg, Charlie Quinn, and Naresh Doni Jayavelu for assistance with statistical analyses; and the Pepper, Campbell, and Chu labs for helpful discussion. Figure cartoon created with BioRender.com. This work was supported by the following funding: L.B.R. and K.B.P. (NIH2T32 AI106677); U. Washington Cell Analysis Facility, Symphony A3 NIH 1S10OD024979-01A1; D.J.C. and P.A.M. (NIH R01AI127726, NIH U19AI125378-S1), and M.P. (NIH U01AI142001-02S1; R01AI118803); BWF #1018486 and COVID Pilot grant to M.P.; and Emergent Ventures fast grant to M.P.

AUTHOR CONTRIBUTIONS

M.P., L.B.R., K.B.P., D.J.C., and P.A.M. conceived the study. M.P., H.Y.C., M.G., and L.B.R. initiated and ran the clinical studies. N.F., J.L., and C.A.H. enrolled participants, managed surveys, and coordinated visits. C.S. and I.G. procured samples. C.A.H., L.B.R., N.F., and J.L. processed and preserved blood and plasma samples. L.B.R. generated and validated tetramer reagents. M.H. generated pseudoviruses. L.B.R. and C.A.H. performed enzyme-linked immunosorbent assay (ELISA) experiments. J.E. performed plaque reduction neutralization test (PRNT) experiments. L.B.R. performed and analyzed antigen-specific B cell flow cytometry and pseudovirus neutralization test (pVNT) experiments. D.J.C. defined SARS-CoV-2 peptide pool construction. P.A.M. and K.B.P. conceived, performed, and analyzed AIM T cell experiments with help from M.L.F. L.B.R., P.A.M., K.B.P., D.J.C., and M.P. drafted the manuscript. All authors helped edit the manuscript. M.P. secured funds and supervised the project.

DECLARATION OF INTERESTS

M.P. is a member of the Scientific Advisory Board of VaxArt and NeoLeukin Inc.

INCLUSION AND DIVERSITY

We worked to ensure gender balance in the recruitment of human subjects. We worked to ensure that the study questionnaires were prepared in an inclusive way. One or more of the authors of this paper self-identifies as an underrepresented ethnic minority in science.

Received: January 13, 2022
Revised: February 23, 2022
Accepted: March 14, 2022
Published: March 17, 2022

REFERENCES

Abu-Raddad, L.J., Chemaitelly, H., Ayoub, H.H., Yassine, H.M., Benslimane, F.M., Khatib, H.A.A., Tang, P., Hasan, M.R., Coyle, P., Kanaani, Z.A., et al. (2021). Protection afforded by the BNT162b2 and mRNA-1273 COVID-19 vaccines in fully vaccinated cohorts with and without prior infection. Preprint at medRxiv. 2021.07.25.21261093.

Baden, L.R., Sahly, H.M.E., Essink, B., Kotloff, K., Frey, S., Novak, R., Diemert, D., Spector, S.A., Rouphael, N., Creech, C.B., et al. (2020). Efficacy and safety of the mRNA-1273 SARS-CoV-2 vaccine. N. Engl. J. Med. *384*, 403–416.

Becht, E., Tolstrup, D., Dutertre, C.-A., Morawski, P.A., Campbell, D.J., Ginhoux, F., Newell, E.W., Gottardo, R., and Headley, M.B. (2021). High-throughput single-cell quantification of hundreds of proteins using conventional flow cytometry and machine learning. Sci. Adv. *7*, eabg0505.

Brinkmann, V., Geiger, T., Alkan, S., and Heusser, C.H. (1993). Interferon alpha increases the frequency of interferon gamma-producing human CD4+ T cells. J. Exp. Med. *178*, 1655–1663.

Cameroni, E., Bowen, J.E., Rosen, L.E., Saliba, C., Zepeda, S.K., Culap, K., Pinto, D., VanBlargan, L.A., Marco, A.D., di Iulio, J., et al. (2021). Broadly neutralizing antibodies overcome SARS-CoV-2 Omicron antigenic shift. Nature *602*, 664–670.

Cancro, M.P., and Tomayko, M.M. (2021). Memory B cells and plasma cells: the differentiative continuum of humoral immunity. Immunol. Rev. *303*, 72–82.

Cho, A., Muecksch, F., Schaefer-Babajew, D., Wang, Z., Finkin, S., Gaebler, C., Ramos, V., Cipolla, M., Mendoza, P., Agudelo, M., et al. (2021). Anti-SARS-CoV-2 receptor-binding domain antibody evolution after mRNA vaccination. Nature *600*, 517–522.

Collier, D.A., De Marco, A.D., Ferreira, I.A.T.M., Meng, B., Datir, R.P., Walls, A.C., Kemp, S.A., Bassi, J., Pinto, D., Silacci-Fregni, C., et al. (2021). Sensitivity of SARS-CoV-2 B.1.1.7 to mRNA vaccine-elicited antibodies. Nature *593*, 136–141.

Corbett, K.S., Nason, M.C., Flach, B., Gagne, M., O'Connell, S., Johnston, T.S., Shah, S.N., Edara, V.V., Floyd, K., Lai, L., et al. (2021). Immune correlates of protection by mRNA-1273 vaccine against SARS-CoV-2 in nonhuman primates. Science *373*, eabj0299.

Crawford, K.H.D., Eguia, R., Dingens, A.S., Loes, A.N., Malone, K.D., Wolf, C.R., Chu, H.Y., Tortorici, M.A., Veesler, D., Murphy, M., et al. (2020). Protocol and reagents for pseudotyping lentiviral particles with SARS-CoV-2 spike protein for neutralization assays. Viruses *12*, 513.

Crotty, S. (2021). Hybrid immunity. Science *372*, 1392–1393.

Dan, J.M., Mateus, J., Kato, Y., Hastie, K.M., Yu, E.D., Faliti, C.E., Grifoni, A., Ramirez, S.I., Haupt, S., Frazier, A., et al. (2021). Immunological memory to SARS-CoV-2 assessed for up to 8 months after infection. Science *371*, eabf4063.

De Waal Malefyt, R., Abrams, J., Bennett, B., Figdor, C.G., and de Vries, J.E. (1991). Interleukin 10 (IL-10) inhibits cytokine synthesis by human monocytes: an autoregulatory role of IL-10 produced by monocytes. J. Exp. Med. *174*, 1209–1220.

Erasmus, J.H., Khandhar, A.P., O'Connor, M.A., Walls, A.C., Hemann, E.A., Murapa, P., Archer, J., Leventhal, S., Fuller, J.T., Lewis, T.B., et al. (2020). An Alphavirus-derived replicon RNA vaccine induces SARS-CoV-2 neutralizing antibody and T cell responses in mice and nonhuman primates. Sci. Transl. Med. *12*, eabc9396.

Feng, S., Phillips, D.J., White, T., Sayal, H., Aley, P.K., Bibi, S., Dold, C., Fuskova, M., Gilbert, S.C., Hirsch, I., et al. (2021). Correlates of protection against symptomatic and asymptomatic SARS-CoV-2 infection. Nat. Med. *27*, 2032–2040.

Fonseca, R., Beura, L.K., Quarnstrom, C.F., Ghoneim, H.E., Fan, Y., Zebley, C.C., Scott, M.C., Fares-Frederickson, N.J., Wijeyesinghe, S., Thompson, E.A., et al. (2020). Developmental plasticity allows outside-in immune responses by resident memory T cells. Nat. Immunol. *21*, 412–421.

Gabryšová, L., Alvarez-Martinez, M., Luisier, R., Cox, L.S., Sodenkamp, J., Hosking, C., Pérez-Mazliah, D., Whicher, C., Kannan, Y., Potempa, K., et al. (2018). c-Maf controls immune responses by regulating disease-specific gene networks and repressing IL-2 in CD4+ T cells. Nat. Immunol. *19*, 497–507.

Galani, I.-E., Rovina, N., Lampropoulou, V., Triantafyllia, V., Manioudaki, M., Pavlos, E., Koukaki, E., Fragkou, P.C., Panou, V., Rapti, V., et al. (2021). Untuned antiviral immunity in COVID-19 revealed by temporal type I/III interferon patterns and flu comparison. Nat. Immunol. *22*, 32–40.

Gazit, S., Shlezinger, R., Perez, G., Lotan, R., Peretz, A., Ben-Tov, A., Cohen, D., Muhsen, K., Chodick, G., and Patalon, T. (2021). Comparing SARS-CoV-2 natural immunity to vaccine-induced immunity: reinfections versus breakthrough infections. Preprint at Medrxiv. 2021.08.24.21262415.

Gazzinelli, R.T., Wysocka, M., Hieny, S., Scharton-Kersten, T., Cheever, A., Kühn, R., Müller, W., Trinchieri, G., and Sher, A. (1996). In the absence of endogenous IL-10, mice acutely infected with Toxoplasma gondii succumb to a lethal immune response dependent on CD4+ T cells and accompanied by overproduction of IL-12, IFN-gamma and TNF-alpha. J. Immunol. *157*, 798–805.

Gilbert, P.B., Montefiori, D.C., McDermott, A.B., Fong, Y., Benkeser, D., Deng, W., Zhou, H., Houchens, C.R., Martins, K., Jayashankar, L., et al. (2022). Immune correlates analysis of the mRNA-1273 COVID-19 vaccine efficacy clinical trial. Science *375*, 43–50.

Glass, D.R., Tsai, A.G., Oliveria, J.P., Hartmann, F.J., Kimmey, S.C., Calderon, A.A., Borges, L., Glass, M.C., Wagar, L.E., Davis, M.M., and Bendall, S.C. (2020). An integrated multi-omic single-cell atlas of human B cell identity. Immunity *53*, 217–232.e5.

Goel, R.R., Painter, M.M., Apostolidis, S.A., Mathew, D., Meng, W., Rosenfeld, A.M., Lundgreen, K.A., Reynaldi, A., Khoury, D.S., Pattekar, A., et al. (2021). mRNA vaccines induce durable immune memory to SARS-CoV-2 and variants of concern. Science *374*, abm0829.

Goldberg, Y., Mandel, M., Bar-On, Y.M., Bodenheimer, O., Freedman, L., Ash, N., Alroy-Preis, S., Huppert, A., and Milo, R. (2021). Protection and waning of natural and hybrid COVID-19 immunity. Preprint at medRxiv. 2021.12.04.21267114.

Guerrera, G., Picozza, M., D'Orso, S., Placido, R., Pirronello, M., Verdiani, A., Termine, A., Fabrizio, C., Giannessi, F., Sambucci, M., et al. (2021). BNT162b2 vaccination induces durable SARS-CoV-2 specific T cells with a stem cell memory phenotype. Sci. Immunol. *6*, eabl5344.

Hunter, C.A., Ellis-Neyes, L.A., Slifer, T., Kanaly, S., Griinig, G., Fort, M., Rennick, D., and Araujot, F.G. (1997). 1L-10 is required to prevent immune hyperactivity During infection with Trypanosoma cruzi. J. Immunol. *158*, 3311–3316.

Jankovic, D., Kullberg, M.C., Feng, C.G., Goldszmid, R.S., Collazo, C.M., Wilson, M., Wynn, T.A., Kamanaka, M., Flavell, R.A., and Sher, A. (2007). Conventional T-bet+Foxp3− Th1 cells are the major source of host-protective regulatory IL-10 during intracellular protozoan infection. J. Exp. Med. *204*, 273–283.

Khoury, D.S., Cromer, D., Reynaldi, A., Schlub, T.E., Wheatley, A.K., Juno, J.A., Subbarao, K., Kent, S.J., Triccas, J.A., and Davenport, M.P. (2021). Neutralizing antibody levels are highly predictive of immune protection from symptomatic SARS-CoV-2 infection. Nat. Med. *27*, 1205–1211.

Kim, C.C., Baccarella, A.M., Bayat, A., Pepper, M., and Fontana, M.F. (2019). FCRL5+ memory B cells exhibit robust recall responses. Cell Rep. *27*, 1446–1460.e4.

Kim, W., Zhou, J.Q., Sturtz, A.J., Horvath, S.C., Schmitz, A.J., Lei, T., Kalaidina, E., Thapa, M., Alsoussi, W.B., Haile, A., et al. (2021). Germinal centre-driven maturation of B cell response to SARS-CoV-2 vaccination. Preprint at bioRxiv. 2021.10.31.466651.

Klicznik, M.M., Morawski, P.A., Höllbacher, B., Varkhande, S.R., Motley, S.J., Kuri-Cervantes, L., Goodwin, E., Rosenblum, M.D., Long, S.A., Brachtl, G., et al. (2019). Human CD4+CD103+ cutaneous resident memory T cells are found in the circulation of healthy individuals. Sci. Immunol. *4*, eaav8995.

Knox, J.J., Kaplan, D.E., and Betts, M.R. (2017). T-bet-expressing B cells during HIV and HCV infections. Cell. Immunol. *321*, 26–34.

Krishnamurty, A.T., Thouvenel, C.D., Portugal, S., Keitany, G.J., Kim, K.S., Holder, A., Crompton, P.D., Rawlings, D.J., and Pepper, M. (2016). Somatically hypermutated Plasmodium-specific IgM+ memory B cells are rapid, plastic, early responders upon malaria rechallenge. Immunity *45*, 402–414.

Laidlaw, B.J., and Ellebedy, A.H. (2022). The germinal centre B cell response to SARS-CoV-2. Nat. Rev. Immunol. *22*, 7–18.

Lazarevic, V., Glimcher, L.H., and Lord, G.M. (2013). T-bet: a bridge between innate and adaptive immunity. Nat. Rev. Immunol. *13*, 777–789.

Le Bert, N., Clapham, H.E., Tan, A.T., Chia, W.N., Tham, C.Y.L., Lim, J.M., Kunasegaran, K., Tan, L.W.L., Dutertre, C.-A., Shankar, N., et al. (2021). Highly functional virus-specific cellular immune response in asymptomatic SARS-CoV-2 infection. J. Exp. Med. *218*, e20202617.

Levine, J.H., Simonds, E.F., Bendall, S.C., Davis, K.L., Amir, E.-D., Tadmor, M.D., Litvin, O., Fienberg, H.G., Jager, A., Zunder, E.R., et al. (2015). Data-driven phenotypic dissection of AML reveals progenitor-like cells that correlate with prognosis. Cell *162*, 184–197.

Lucas, C., Wong, P., Klein, J., Castro, T.B.R., Silva, J., Sundaram, M., Ellingson, M.K., Mao, T., Oh, J.E., Israelow, B., et al. (2020). Longitudinal analyses reveal immunological misfiring in severe COVID-19. Nature *584*, 463–469.

O'Garra, A., and Vieira, P. (2007). TH1 cells control themselves by producing interleukin-10. Nat. Rev. Immunol. *7*, 425–428.

Olatunde, A.C., Hale, J.S., and Lamb, T.J. (2021). Cytokine-skewed Tfh cells: functional consequences for B cell help. Trends Immunol. *42*, 536–550.

Painter, M.M., Mathew, D., Goel, R.R., Apostolidis, S.A., Pattekar, A., Kuthuru, O., Baxter, A.E., Herati, R.S., Oldridge, D.A., Gouma, S., et al. (2021). Rapid induction of antigen-specific CD4+ T cells is associated with coordinated humoral and cellular immunity to SARS-CoV-2 mRNA vaccination. Immunity *54*, 2133–2142.e3.

Pape, K.A., Dileepan, T., Kabage, A.J., Kozysa, D., Batres, R., Evert, C., Matson, M., Lopez, S., Krueger, P.D., Graiziger, C., et al. (2021). High-affinity memory B cells induced by SARS-CoV-2 infection produce more plasmablasts and atypical memory B cells than those primed by mRNA vaccines. Cell Rep. *37*, 109823. https://doi.org/10.1016/j.celrep.2021.109823.

Payne, R.P., Longet, S., Austin, J.A., Skelly, D.T., Dejnirattisai, W., Adele, S., Meardon, N., Faustini, S., Al-Taei, S., Moore, S.C., et al. (2021). Immunogenicity of standard and extended dosing intervals of BNT162b2 mRNA vaccine. Cell *184*, 5699–5714.e11.

Polack, F.P., Thomas, S.J., Kitchin, N., Absalon, J., Gurtman, A., Lockhart, S., Perez, J.L., Pérez Marc, G.P., Moreira, E.D., Zerbini, C., et al. (2020). Safety and efficacy of the BNT162b2 mRNA Covid-19 vaccine. N. Engl. J. Med. *383*, 2603–2615.

Poon, M.M.L., Rybkina, K., Kato, Y., Kubota, M., Matsumoto, R., Bloom, N.I., Zhang, Z., Hastie, K.M., Grifoni, A., Weiskopf, D., et al. (2021). SARS-CoV-2 infection generates tissue-localized immunological memory in humans. Sci. Immunol. *6*, eabl9105.

Pot, C., Jin, H., Awasthi, A., Liu, S.M., Lai, C.-Y., Madan, R., Sharpe, A.H., Karp, C.L., Miaw, S.-C., Ho, I.-C., and Kuchroo, V.K. (2009). Cutting edge: il-27 induces the transcription factor c-Maf, cytokine IL-21, and the Costimulatory receptor ICOS that coordinately act together to promote differentiation of IL-10-producing Tr1 cells. J. Immunol. *183*, 797–801.

Reiss, S., Baxter, A.E., Cirelli, K.M., Dan, J.M., Morou, A., Daigneault, A., Brassard, N., Silvestri, G., Routy, J.-P., Havenar-Daughton, C., et al. (2017). Comparative analysis of activation induced marker (AIM) assays for sensitive identification of antigen-specific CD4 T cells. PLoS One *12*, e0186998.

Reynolds, C.J., Pade, C., Gibbons, J.M., Butler, D.K., Otter, A.D., Menacho, K., Fontana, M., Smit, A., Sackville-West, J.E., Cutino-Moguel, T., et al. (2021). Prior SARS-CoV-2 infection rescues B and T cell responses to variants after first vaccine dose. Science *372*, 1418–1423.

Rodda, L.B., Netland, J., Shehata, L., Pruner, K.B., Morawski, P.A., Thouvenel, C.D., Takehara, K.K., Eggenberger, J., Hemann, E.A., Waterman, H.R., et al. (2021). Functional SARS-CoV-2-Specific immune memory persists after mild COVID-19. Cell *184*, 169–183.e17.

Ruterbusch, M., Pruner, K.B., Shehata, L., and Pepper, M. (2020). *In vivo* CD4+ T cell differentiation and function: revisiting the Th1/Th2 paradigm. Annu. Rev. Immunol. *38*, 705–725.

Schmidt, F., Muecksch, F., Weisblum, Y., Da Silva, J., Bednarski, E., Cho, A., Wang, Z., Gaebler, C., Caskey, M., Nussenzweig, M.C., et al. (2021a). Plasma neutralization of the SARS-CoV-2 Omicron variant. N. Engl. J. Med. *386*, 599–601.

Schmidt, F., Weisblum, Y., Rutkowska, M., Poston, D., DaSilva, J., Zhang, F., Bednarski, E., Cho, A., Schaefer-Babajew, D.J., Gaebler, C., et al. (2021b).

High genetic barrier to SARS-CoV-2 polyclonal neutralizing antibody escape. Nature *600*, 512–516.

Stamatatos, L., Czartoski, J., Wan, Y.-H., Homad, L.J., Rubin, V., Glantz, H., Neradilek, M., Seydoux, E., Jennewein, M.F., Maccamy, A.J., et al. (2021). mRNA vaccination boosts cross-variant neutralizing antibodies elicited by SARS-CoV-2 infection. Science *372*, eabg9175.

Stolley, J.M., Johnston, T.S., Soerens, A.G., Beura, L.K., Rosato, P.C., Joag, V., Wijeyesinghe, S.P., Langlois, R.A., Osum, K.C., Mitchell, J.S., and Masopust, D. (2020). Retrograde migration supplies resident memory T cells to lung-draining LN after influenza infection. J. Exp. Med. *217*, e20192197.

Sun, J., Madan, R., Karp, C.L., and Braciale, T.J. (2009). Effector T cells control lung inflammation during acute influenza virus infection by producing IL-10. Nat. Med. *15*, 277–284.

Tarke, A., Sidney, J., Kidd, C.K., Dan, J.M., Ramirez, S.I., Yu, E.D., Mateus, J., da Silva Antunes, R.da S., Moore, E., Rubiro, P., et al. (2021). Comprehensive analysis of T cell immunodominance and immunoprevalence of SARS-CoV-2 epitopes in COVID-19 cases. Cell Rep. Med. *2*, 100204.

Tortorici, M.A., Czudnochowski, N., Starr, T.N., Marzi, R., Walls, A.C., Zatta, F., Bowen, J.E., Jaconi, S., Di Iulio, J.D., Wang, Z., et al. (2021). Broad sarbecovirus neutralization by a human monoclonal antibody. Nature *597*, 103–108.

Turner, J.S., Kim, W., Kalaidina, E., Goss, C.W., Rauseo, A.M., Schmitz, A.J., Hansen, L., Haile, A., Klebert, M.K., Pusic, I., et al. (2021a). SARS-CoV-2 infection induces long-lived bone marrow plasma cells in humans. Nature *595*, 421–425.

Turner, J.S., O'Halloran, J.A., Kalaidina, E., Kim, W., Schmitz, A.J., Zhou, J.Q., Lei, T., Thapa, M., Chen, R.E., Case, J.B., et al. (2021b). SARS-CoV-2 mRNA vaccines induce persistent human germinal centre responses. Nature *596*, 109–113.

Ueno, H. (2016). Human circulating T follicular helper cell subsets in health and disease. J. Clin. Immunol. *36* (*Suppl. 1*), 34–39.

Walls, A.C., Fiala, B., Schäfer, A., Wrenn, S., Pham, M.N., Murphy, M., Tse, L.V., Shehata, L., O'Connor, M.A., Chen, C., et al. (2020). Elicitation of potent neutralizing antibody responses by designed protein nanoparticle vaccines for SARS-CoV-2. Cell *183*, 1367–1382.e17.

Wang, Z., Muecksch, F., Schaefer-Babajew, D., Finkin, S., Viant, C., Gaebler, C., Hoffmann, H.-H., Barnes, C.O., Cipolla, M., Ramos, V., et al. (2021). Naturally enhanced neutralizing breadth against SARS-CoV-2 one year after infection. Nature *595*, 426–431.

Wijeyesinghe, S., Beura, L.K., Pierson, M.J., Stolley, J.M., Adam, O.A., Ruscher, R., Steinert, E.M., Rosato, P.C., Vezys, V., and Masopust, D. (2021). Expansible residence decentralizes immune homeostasis. Nature *592*, 457–462.

Yang, Y., Ochando, J., Yopp, A., Bromberg, J.S., and Ding, Y. (2005). IL-6 plays a unique role in initiating c-Maf expression during early stage of CD4 T cell activation. J. Immunol. *174*, 2720–2729.

Zhao, J., Zhao, J., Mangalam, A.K., Channappanavar, R., Fett, C., Meyerholz, D.K., Agnihothram, S., Baric, R.S., David, C.S., and Perlman, S. (2016). Airway memory CD4+ T cells mediate protective immunity against emerging respiratory coronaviruses. Immunity *44*, 1379–1391.

STAR★METHODS

KEY RESOURCES TABLE

REAGENT or RESOURCE	SOURCE	IDENTIFIER
Antibodies		
Anti-human CCR4-PE/Dazzle594, Clone L291H4	BioLegend	CAT#359420; RRID:AB_2564095
Anti-human CCR6-BV650, Clone G043G3	BioLegend	CAT#353426; RRID:AB_2563869
Anti-human CCR7-BV605, Clone G043H7	BioLegend	CAT#353224; RRID:AB_2561753
Anti-human CD107a BV510, Clone H4A3	BioLegend	CAT#328632; RRID:AB_2562648
Anti-human CD11c-PEDazzle594, Clone 3.9	BioLegend	CAT#301642; RRID:AB_2564083
Anti-human CD127 AlexaFlour 488, Clone AO19D5	BioLegend	CAT#351314; RRID:AB_10898315
Anti-human CD127-PE/Cy7, Clone hIL7Rm21	Becton Dickinson	CAT#560822; RRID:AB_2033938
Anti-human CD134-PerCP/Cy5.5, Clone BerACT35	BioLegend	CAT#350010; RRID:AB_10719224
Anti-human CD137-BV750, Clone 4B4-1	BioLegend	CAT#309844; RRID:AB_2876609
Anti-human CD14 BV711, Clone M5E2	BioLegend	CAT#301838; RRID:AB_2562909
Anti-human CD14-PerCP/Cy5.5, Clone M5E2	BioLegend	CAT#301824; RRID:AB_893251
Anti-human CD154 Biotin, Clone hCD40L-M91	Becton Dickinson	CAT#552560; RRID:AB_394429
Anti-human CD16 BV711, Clone 3G8	Becton Dickinson	CAT#563127; RRID:AB_2732050
Anti-human CD16-PerCP/Cy5.5, Clone 3G8	BioLegend	CAT#302028; RRID:AB_893262
Anti-human CD19 BV711, Clone SJ25C1	Becton Dickinson	CAT#563036; RRID:AB_2737968
Anti-human CD19-APC/Fire810, Clone HIB19	BioLegend	CAT#302271; RRID:AB_2860770
Anti-human CD19-BUV496, Clone SJ25C1	Becton Dickinson	CAT#612939; RRID:AB_2870221
Anti-human CD20-BV711, Clone 2H7	BioLegend	CAT#302341; RRID:AB_2562601
Anti-human CD21-SB600 Clone, HB5	Thermo Fisher	CAT#63-0219-41; RRID:AB_2744835
Anti-human CD25 BV650, Clone M-A251	Becton Dickinson	CAT#563719; RRID:AB_2744337
Anti-human CD25-PE/Cy5, Clone BC96	BioLegend	CAT#302608; RRID:AB_314278
Anti-human CD26-BUV805, Clone M-A261	Becton Dickinson	CAT#749316; RRID:AB_2873690
Anti-human CD27-BV421, Clone M-T271	BioLegend	CAT#356418; RRID:AB_2562599
Anti-human CD27-BV711, Clone M-T271	BioLegend	CAT#356430; RRID:AB_2650751
Anti-human CD3 eFluor450, Clone OKT3	Thermo Fisher	CAT#48-0037-42; RRID:AB_1272055
Anti-human CD3-BUV615, Clone UCHT1	Becton Dickinson	CAT#612993; RRID:AB_2870264
Anti-human CD3-PerCP/Cy5.5, Clone HIT3a	BioLegend	CAT#300328; RRID:AB_1575008
Anti-human CD38-AF700, Clone HIT2	Thermo Fisher	CAT#56-0381-82; RRID:AB_657740
Anti-human CD4 Alexa Flour 700, Clone RPA-T4	Becton Dickinson	CAT#557922; RRID:AB_396943
Anti-human CD4-SparkNIR685, Clone SK3	BioLegend	CAT#344657; RRID:AB_2819980
Anti-human CD45-Ax532, Clone HI30	Thermo Fisher	CAT#58-0459-42; RRID:AB_11218673
Anti-human CD45-BUV395, Clone HI30	Becton Dickinson	CAT#563792; RRID:AB_2869519
Anti-human CD45-BUV496, Clone HI30	Becton Dickinson	CAT#750179; RRID:AB_2868405
Anti-human CD45-e450, Clone HI30	Thermo Fisher	CAT#48-0459-42; RRID:AB_2016677
Anti-human CD45RA BV711, Clone HI100	Becton Dickinson	CAT#563733; RRID:AB_2738392
Anti-human CD45RA-BUV737, Clone HI100	Becton Dickinson	CAT#612847; RRID:AB_2833053
Anti-human CD57-BV785, Clone QA17A04	BioLegend	CAT#393329; RRID:AB_2860967
Anti-human CD69-APC/R700, Clone FN50	Becton Dickinson	CAT#565154; RRID:AB_2744449
Anti-human CD69-BUV395, Clone FN50	Becton Dickinson	CAT#564364; RRID:AB_2738770
Anti-human CD8 PE/Cy5, Clone RPA-T8	Becton Dickinson	CAT#555368; RRID:AB_395771
Anti-human CD8-BV480, Clone RPA-T8	Becton Dickinson	CAT#566163; RRID:AB_2739560
Anti-human CXCR3-BV421, Clone G025H7	BioLegend	CAT#353716; RRID:AB_2561448
Anti-human CXCR5 Alexa Flour 647, Clone J252D4	BioLegend	CAT#356906; RRID:AB_2561815

(*Continued on next page*)

Continued

REAGENT or RESOURCE	SOURCE	IDENTIFIER
Anti-human CXCR5-BB515, Clone RF8B2	Becton Dickinson	CAT#564624; RRID:AB_2738871
Anti-human gamma/delta TCR-APC/Fire750, Clone B1	BioLegend	CAT#331228; RRID:AB_2650627
Anti-human HLA-DR-BUV661, Clone G46-6	Becton Dickinson	CAT#612981; RRID:AB_2870252
Anti-human ICOS-APC, Clone C398.4a	BioLegend	CAT#313509; RRID:AB_416333
Anti-human IFNy APCeF780, Clone 4s-B3	Thermo Fisher	CAT#47-7319-42; RRID:AB_10853011
Anti-human IgA-Biotin, Clone IS11-8E10	Miltenyi Biotech	CAT#130-113-474; RRID:AB_2733547
anti-human IgA-HRP	Southern Biotech	CAT#2050-05; RRID:AB_2687526
Anti-human IgA-PE-Vio 770, Clone IS11-8E10	Miltenyi Biotech	CAT#130-114-003; RRID:AB_2751180
Anti-human IgD-BUV395, Clone IA6-2	Becton Dickinson	CAT#563813; RRID:AB_2738435
Anti-human IgG-BV786, Clone G18-145	Becton Dickinson	CAT#564230; RRID:AB_2738684
Anti-human IgG-HRP	Jackson ImmunoResearch	CAT#109-035-088; AB_2337584
Anti-human IgM-BV510, Clone MHM-88	BioLegend	CAT#314521; RRID:AB_2561513
Anti-human IL-10 PE Dazzle 594, Clone JES3-9D7	BioLegend	CAT#501426; RRID:AB_2566744
Anti-human IL-13 BV421, Clone JES10-5E2	BioLegend	CAT#501916; RRID:AB_2616748
Anti-human IL-17A BV570, Clone BL168	BioLegend	CAT#512324; RRID:AB_2563886
Anti-human IL-2 BV785, Clone MQ1-17H12	BioLegend	CAT#500348; RRID:AB_2566471
Anti-human IL-21 PE, Clone 3A3-N2	Thermo Fisher	CAT#12-7219-42; RRID:AB_1582260
Anti-human IL-4 PECy7, Clone MP4-25D2	BioLegend	CAT#500824; RRID:AB_2126746
Anti-human PD-L1-PE, Clone 29E.2A3	BioLegend	CAT#329705; RRID:AB_940366
Bacterial and virus strains		
SARS-CoV-2 (WA-1)	BEI resources	NR-52281
Biological samples		
Human PBMC	This paper	N/A
Human Plasma	This paper	N/A
Chemicals, peptides, and recombinant proteins		
1X 3,3′,5,5′-Tetramethylbenzidine (TMB)	Invitrogen	CAT#00-4201-56
anti-CD40 agonist mAb	Miltenyi Biotec	CAT#130-094-133; RRID:AB_10839704
anti-PE magnetic beads	Miltenyi Biotec	CAT#130-048-801; RRID:AB_244373
Avicel RC-591	FMC	CAT#Avicel RC-591
BirA500 kit	Avidity	CAT#BirA500
Bright-Glo Luciferase Assay System luciferase	Promega	CAT#E2610
CEFX Ultra SuperStim Pool	JPT	CAT#PM-CEFX-2
Crystal Violet	Milipore Sigma	CAT#V5265
Decoy Tetramer APC-Dy755	This paper	N/A
Decoy Tetramer PE-Dy594-Dy650	This paper	N/A
DMSO, Cell culture grade >99.5%	Sigma-Aldrich	CAT#D4540
Dylight NHS Ester 594	Thermo Fisher	CAT#46413
Dylight NHS Ester 650	Thermo Fisher	CAT#62266
Dylight NHS Ester 755	Thermo Fisher	CAT#84538
Fixable Live Dead BLUE BUV496	Thermo Scientific	CAT#L23105
Fixation/Permeabilization kit	Becton Dickinson	CAT#554714
GolgiStop/monensin	Becton Dickinson	CAT#554724
Ionomycin	Sigma-Aldrich	CAT#I9657
Paraformaldahyde solution, 4% in PBS	Thermo Scientific	CAT#AAJ19943K2
phorbol 12-myristate 13-acetate	Sigma-Aldrich	CAT#P8139
poly-L-lysine	Milipore Sigma	CAT#P4707
RBD(Wu-1) Tetramer APC	This paper	N/A

(*Continued on next page*)

Continued		
REAGENT or RESOURCE	SOURCE	IDENTIFIER
RBD(Wu-1) Tetramer PE	This paper	N/A
Recombinant SARS-CoV-2 (Wuhan-1) RBD protein	Walls et al., 2020	N/A
Recombinant SARS-CoV-2 RBD (B.1.1.351, β) protein	This paper	N/A
SARS-CoV-2 HLA Class I & II 15-mer peptides: Membrane	BEI Resources	NR-52403
SARS-CoV-2 HLA Class I & II 15-mer peptides: Spike	BEI Resources	NR-52402
Streptavidin BV605, Clone 563260	Becton Dickinson	CAT#563260; RRID:AB_2869476
Streptavidin-APC	Agilent	CAT#PJ27S-1
Streptavidin-BUV805	Becton Dickinson	CAT#564923; RRID:AB_2869629
Streptavidin-PE	Agilent	CAT#PJRS301-1
UltraComp eBeads Compensation Beads	Thermo Fisher	CAT#01-2222-42
Zombie LiveDead NIR	BioLegend	CAT#423105
Critical commercial assays		
NEBuilder HiFi DNA Assembly	New England Biolabs	CAT#E5520S
Experimental models: Cell lines		
293T	ATCC	ACS-4500
human ACE2-293T	BEI Resources	NR-52511
Recombinant DNA		
CMV.Luc.IRES.GFP vector plasmid	BEI Resources	NR52516
CMVR. SARS-CoV-2-Beta-RBD-Avi (K417N-E484K-N501Y) plasmid	This paper, GenScript	N/A
pHDM vector with SARS-CoV-2(Wu-1), D614G with C-Term. Del.	BEI Resources	NR-53765
pMD2.g plasmid	Didier Trono; Addgene	CAT#12260
SARS-CoV-2(o)-spike pseudotyping plasmid	This paper	N/A
SARS-CoV-2(Δ)-spike pseudotyping plasmid	Invivogen	pLV-Spike-V8
Software and algorithms		
FlowJo10	Becton Dickinson	N/A
MikroWin 2000	MikroWin 2000	N/A
Prism	GraphPad	N/A
R	R core team	N/A
SpectroFlo	Cytek Biosciences	N/A

RESOURCE AVAILABILITY

Lead contact

Requests for further information and reagents should be directed to and will be fulfilled by Marion Pepper (mpepper@uw.edu).

Materials availability

Unique tetramer reagents generated in this study are available upon reasonable request.

Data and code availability

- All data reported in this paper will be shared by the lead contact upon request.
- This paper does not report original code.
- Any additional information required to reanalyze the data reported in this paper is available from the lead contact upon request.

EXPERIMENTAL MODEL AND SUBJECT DETAILS

Ethics statement

Participants were enrolled in the Hospitalized or Ambulatory Adults with Respiratory Viral Infections (HAARVI) study (STUDY00000959), Healthy Adult Specimen Repository study (STUDY00002929) or COVID-19/SARS-CoV-2 Prevalence and Antibody Therapy

Development study (Gale Lab, STUDY00009810). All studies are approved by the University of Washington Human Subjects Division Institutional Review Board. Informed consent was obtained from all enrolled participants. Samples were de-identified prior to analysis.

Human study participants and clinical data

Participants were enrolled in one of three prospective cohort studies for longitudinal tracking of immune responses to COVID-19 vaccination in WA, USA. Cohort details are reported in Table 1. Previously SARS-CoV-2 infected (PI) individuals reported a positive SARS-CoV-2 PCR nasal swab or in one case a positive antibody test within 3 months of symptom onset in 2/2020- 10/2020. PI individuals reported mildly symptomatic disease not requiring hospitalization. Participants were considered SARS-CoV-2 naive (N) prior to vaccination based on no prior positive SARS-CoV-2 PCR nasal swab and no detectable SARS-CoV-2 RBD IgG by ELISA (below a threshold of mean + 3 standard deviations of historical negative plasma samples drawn prior to 2020). All participants completed surveys regarding symptom and demographic information. Blood draws were collected pre-vaccination (N: 21, PI: 23), 1 week post-vaccination 2 (N: 18, PI: 22), 3 months post-vaccination 2 (N: 15, PI: 23), 6 months post-vaccination 2 (N: 8, PI: 9) and 2 weeks post-vaccination 3 (N: 8, PI: 10). Not all samples were run for both plasma and PBMC assessments.

Cell lines

Unless otherwise noted, cell lines were cultured in DMEM with 10% heat-inactivated FBS, 2 mM L-glutamine, 10mM HEPES, 100 U/mL penicillin, and 100 μg/mL streptomycin in a humidified atmosphere with 5% CO_2 at 37°C.

METHOD DETAILS

Sample processing and plasma collection

Venous blood from study volunteers was collected in EDTA tubes and spun at 700 x g for 10 min. Plasma was collected, heat-inactivated at 56°C for 30 min and stored at -80°C. Cellular fraction was resuspended in phosphate buffered saline (PBS) and PBMCs were separated from red blood cells using Sepmate PBMC Isolation Tubes (STEMCELL Technologies) according to manufacturer's instruction or cells were resuspended in HBSS, washed, overlaid with ficoll, spun at 400 x g for 30 min with no brake and PBMCs collected. Cells were washed twice in HBSS and frozen at -80°C before being stored in liquid nitrogen.

SARS-CoV-2 RBD protein and tetramer generation

Recombinant SARS-CoV-2 RBD (Wuhan-1, Wu-1) was generated by standard transient transfection followed by IMAC purification as described previously (Walls et al., 2020). Recombinant SARS-CoV-2 RBD (B.1.1.351, β) was generated by transient transfection from the SARS-CoV-2-Beta-RBD-Avi (K417N-E484K-N501Y) construct synthesized by GenScript into CMVR with an N-terminal mu-phosphatase signal peptide and a C-terminal octa-histidine tag, flexible linker, and avi tag (GHHHHHHHHGGSSGLNDIFEAQKIEWHE) as described previously (Tortorici et al., 2021). For tetramer generation, RBD proteins were biotinylated with the BirA500 kit (Avidity), tetramerized with streptavidin-phycoerythrin (SA-PE) or streptavidin-allophycocyanin (SA-APC) (Agilent) and stored in 50% glycerol at -20°C as previously described (Krishnamurty et al., 2016). Decoy reagents were generated by tetramerizing an irrelevant biotinylated protein with SA-PE previously conjugated to Dylight594 NHS Ester (ThermoFisher) and Dylight650 NHS Ester (ThermoFisher) or SA-APC previously conjugated to Dylight755 NHS Ester (ThermoFisher).

Enzyme-linked immunosorbent assay (ELISA)

96-well plates (Corning) were coated with 2 ug/mL of recombinant SARS-CoV-2 RBD protein diluted in PBS and incubated at 4°C overnight. Plates were washed with PBS-T (PBS containing 0.05% Tween-20) and incubated with blocking buffer (PBS-T and 3% milk) for 1h at room temperature (RT). Plasma, culture supernatants or monoclonal antibodies were serially diluted in dilution buffer (PBS-T and 1% milk) in triplicate, added to plates, and incubated at RT for 2 h. Secondary antibodies were diluted in dilution buffer as follows: anti-human IgG-HRP (Jackson ImmunoResearch) at 1:3000 or anti-human IgA-HRP (Southern Biotech) at 1:1500. Plates were incubated with secondary antibodies for 1h at RT, then detected with 1X 3,30,5,50-Tetramethylbenzidine (TMB) (Invitrogen) and quenched with 1M HCl. Sample optical density (OD) was measured by a spectrophotometer at 450 nm and 570 nm.

SARS-CoV-2 spike pseudotyped lentivirus

The SARS-CoV-2(o)-spike pseudotyping plasmid was assembled by introducing gene fragments synthesized by Integrated DNA Technologies (Coralville, IA, USA) encoding the SARS-CoV-2(o) variant (B.1.1.529, Omicron) spike gene to replace the Wu-Spike_D614G sequence in a digested pseudotyping plasmid backbone (BEI Resources; NR-53765) using standard molecular biology techniques, including NEBuilder HiFi DNA Assembly (New England Biolabs, Ipswich, MA, USA). Plasmid sequence was confirmed by Sanger sequencing. The SARS-CoV-2(o)- and SARS-CoV-2(Δ)-spike pseudotyped lentiviral vectors (LVs) were each produced by transient polyethylenimine transfection of 293T cells with a CMV.Luc.IRES.GFP vector plasmid (BEI Resources; NR52516), a second generation helper plasmid pMD2.g (gift from Didier Trono; Addgene #12260), and either: the SARS-CoV-2(o) pseudotyping plasmid above, or a plasmid encoding the SARS-CoV-2(Δ) variant spike (Invivogen, San Diego, CA,USA;

pLV-Spike-V8, B.1.617.2, delta). At 24 hours following transfection, cell culture media was exchanged for fresh DMEM with 3% FCS. Supernatants were harvested the next day, filtered through 0.2uM filters, and concentrated by overnight centrifugation at 4°C. Pellets were then resuspended in PBS at 100X.

Pseudovirus neutralization test (pVNT)

PVNT assays were performed as previously described (Crawford et al., 2020). Briefly, heat inactivated plasma was diluted 1:5 followed by four 3-fold serial dilutions all in duplicate and mixed 1:1 with 10^6 relative luciferase units of SARS-CoV-2(Δ)-spike or SARS-CoV-2(o)-spike pseudotyped lentivirus in DMEM with 10% heat-inactivated FBS, 2 mM L-glutamine, 100 U/mL penicillin, and 100 μg/mL streptomycin. After 1 hour incubation at 37°C, the plasma/virus mixtures were added to 96-well poly-L-lysine-coated plates seeded with human ACE2-expressing 293T cells (BEI Resources: NR-52511) 20 hours prior. Each plate contained wells with no plasma and wells with no plasma and 293T cells as a background control. After incubating for 48 hours, supernatant was pipet off and replaced with Bright-Glo Luciferase Assay System luciferase (E2610, Promega) for 2 min at 25°C in the dark before transferring to black-bottom plates for measuring luminescence for 1s per well on a Centro LB 960 Microplate Luminometer (Berthold Technologies). Percent neutralization was calculated as (1 – (sample+293T-ACE2+virus RLU - 293T+virus RLU)/(293T-ACE2+virus RLU - 293T+virus RLU) x 100. Data was collected with MikroWin2000 and analyzed in Prism (GraphPad).

Plaque reduction neutralization test (PRNT)

PRNT assays were performed as previously described (Erasmus et al., 2020). Briefly, heat inactivated plasma was diluted 1:5 followed by four 4-fold serial dilutions and mixed 1:1 with 600 PFU/mL SARS-CoV-2 WA-1 (BEI resources; NR-52281) in PBS+0.3% cold water fish skin gelatin (Sigma). After 30 min of incubation at 37°C, the plasma/virus mixtures were added to 12 well plates of Vero cells and incubated for 1 h at 37°C, rocking every 15 min. All dilutions were done in duplicate, along with virus only and no virus controls. Plates were then washed with PBS and overlaid with a 1:1 mixture of 2.4% Avicel RC-591 (FMC) and 2X MEM (ThermoFisher) supplemented with 4% heat-inactivated FBS and Penicillin/Streptomycin (Fisher Scientific.) After a 48h incubation, the overlay was removed, plates were washed with PBS, fixed with 10% formaldehyde (Sigma-Aldrich) in PBS for 30 min at room temp and stained with 1% crystal violet (Sigma-Aldrich) in 20% EtOH. Percent neutralization was calculated as (1 – # sample plaques/# positive control plaques) x 100. Data was analyzed in Prism (GraphPad).

Peptide mesopools

SARS-CoV-2 15-mer peptides, 1mg each (BEI Resources), were provided lyophilized and stored at -80C. Peptides were selected for reactivity against a broad range of class I and class II HLA sub-types for targeted coverage of $CD4^+$ and $CD8^+$ T cell epitopes identified previously (Tarke et al., 2021; Data S1). Before use, peptides were warmed to room temperature for 1 hour then reconstituted in DMSO to a concentration of 10 mg/mL. Individual peptides were combined in equal ratios to create Membrane/Nucleocapsid (182 ug/mL each, 55 peptides) or Spike (200ug/mL each, 49 peptides) megapools, maintaining a total concentration of 10mg/mL.

Activation induced marker assay

Approximately $20x10^6$ PBMC from SARS-CoV-2 naive or previously infected individuals were divided in two for full phenotypic or cytokine analysis. For broad surface phenotyping $10x10^6$ PBMC per sample were further divided into four 5mL polystyrene tubes and cells were pelleted at 250 x g for 5 minutes. Pellets were resuspended at $5x10^6$/mL in one of the following treatment conditions: DMSO (Sigma-Aldrich, >99.5% cell culture grade), 1ug/mL CEFX Ultra SuperStim Pool (JPT, PM-CEFX-2), or 5ug/mL SARS-CoV-2 Membrane and Nucleocapsid or Spike peptide megapools. Stimulation was performed for 18 hours in ImmunoCult-XF T cell Expansion Medium (StemCell Technologies). For intracellular cytokine assessment $2x10^6$/mL PBMC were stimulated using 6.6ug/mL SARS-CoV-2 peptide megapools, or an equivalent volume of DMSO (Sigma-Aldrich, >99.5% cell culture grade) for 12 hours in RPMI complete T cell medium containing anti-human CD40 antagonist mAb (Miltenyi, clone HB10), 5uL LAMP-1/CD107a BV510 mAb (BioLegend, clone H4A3), 2uM CaCl2, and 1.8uL Monensin (Becton Dickinson) - for the final 8 hours of culture.

Immunophenotyping of PBMCs

PBMCs were thawed at 37°C and washed twice before first staining with decoy tetramer and then with RBD tetramer prior to incubation with anti-PE magnetic beads and magnetic bead enrichment (Miltenyi Biotec) as previously described (Krishnamurty et al., 2016). Cells in the positive fraction were stained with surface antibodies for B cell phenotypes. Subsequent analysis of T cells was performed on unlabeled PBMC flow-through resulting from B cell RBD-tetramer pulldown.

PBMC flow-through were stimulated with peptide megapools as described above. For surface phenotyping, cells were washed and barcoded using four different fluorescently labeled CD45 antibodies to create eight unique barcodes as previously described (Becht et al., 2021). Using this method to limit technical variability, all four stimulation conditions for both pre- and post-vaccination samples were combined and fully stained simultaneously for 20 minutes at 37°C. Cells were then fixed for 10 minutes at room temperature using 1% paraformaldehyde (Sigma-Aldrich). For intracellular cytokine staining, cells were first incubated with anti-CXCR5 antibody at room temperature for 40 minutes. Cells were then stained with surface antibodies for 25 minutes at 4°C and then fixed and permeabilized with Fixation/Permeabilization kit (Becton Dickinson) for 15 minutes at room temperature before staining for intracellular cytokines for 20 minutes at room temperature.

Fluorescence flow cytometry

Data were acquired on a five-laser Cytek Aurora (T cell surface phenotyping and T cell intracellular cytokine analysis) or BD FACS Symphony A3 or A5 (B cell surface phenotyping). Control PBMCs or UltraComp eBeads (ThermoFisher) were used for compensation. Up to 10^7 live PBMC were acquired per sample for T cells and all enriched PBMCs were acquired for B cells. Data were analyzed using SpectroFlow (Cytek Biosciences) and FlowJo10 (Becton Dickinson) software.

High-dimensional analysis of cytometry data

AIM-positive ($CD154^+CD69^+$) cells from all data files were concatenated with keywords and subjected to Phenograph clustering algorithm using k=40 nearest neighbors (Levine et al., 2015) and UMAP dimensionality reduction plugins using parameters IL-2, IFN-γ, IL-10, IL-4, IL-21, CD127, CD25, and CXCR5 in FlowJo 10 (Becton Dickinson). Clusters were then enumerated per 10^6 non-naive T cells for each sample by multiplying the percentage ''cluster X parameter'' by percentage ''AIM^+'' and then by 1 million.

QUANTIFICATION AND STATISTICAL ANALYSIS

Statistics

Statistics used are described in figure legends and were determined using Prism (Graphpad). All measurements within a group in a panel are from distinct samples. Data is pooled from nine experiments for Pre and 1w PV2, three experiments for 3m PV2, and two experiments for 2w PV3 time points. Statistical significance of all pairwise comparisons was assessed by two-tailed nonparametric tests; Mann-Whitney for unpaired data and Wilcoxon signed rank tests for paired data except when there were insufficient pairing (less than half of the data set) and then Mann-Whitney was used. No multiple hypothesis testing was applied as the metrics tested were selected based on specific hypotheses.

Supplemental figures

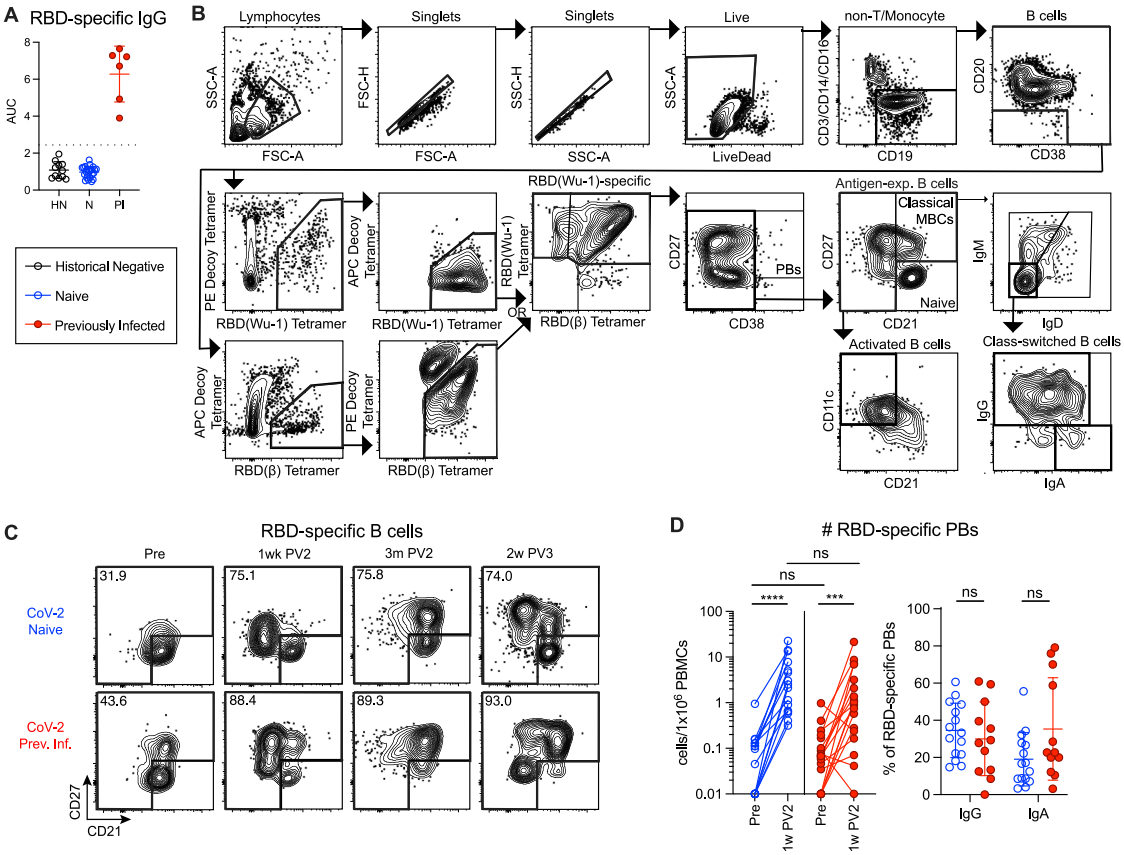

Figure S1. COVID-19 vaccination induces SARS-CoV-2 RBD-specific B cell responses in previously infected and previously naive individuals, related to Figure 1

(A) ELISA area under the curve (AUC) for RBD-specific IgG in plasma collected from individuals prior to 2020 and the SARS-CoV-2 pandemic (historical negatives [HNs], black), SARS-CoV-2 naive (N) individuals and previously infected (PI) individuals that tested PCR$^+$ for SARS-CoV-2. Dashed line indicates mean + 3 SD of HN AUC values.

(B) Representative flow cytometry gates for phenotyping RBD(Wu-1)- and RBD(β)-specific B cells from N and PI PBMCs.

(C) Representative gating on CD19$^+$CD38^{lo}RBD-tetramer$^+$Decoy$^-$ cells for SARS-CoV-2 RBD-specific antigen-experienced (ag-exp.) B cells (CD21$^+$CD27$^+$ and CD21$^-$CD27$^{+/-}$) from N and PI (Prev. Inf.) PBMCs at the indicated time points.

(D) Number (left) and percent IgG$^+$ or IgA$^+$ (right) of RBD-specific plasmablasts (PBs, CD27$^+$CD38^{hi}). Statistics determined by two-tailed Mann-Whitney tests: not significant (ns), *p < 0.05, **p < 0.005, ***p < 0.0005, and ****p < 0.0001. Pre-vaccination (Pre), 1 week post two-dose COVID-19 mRNA vaccination (1w PV2), 3 months post two-dose vaccination (3m PV2), 2 weeks post third vaccination dose (2w PV3). Error bars represent mean and SD.

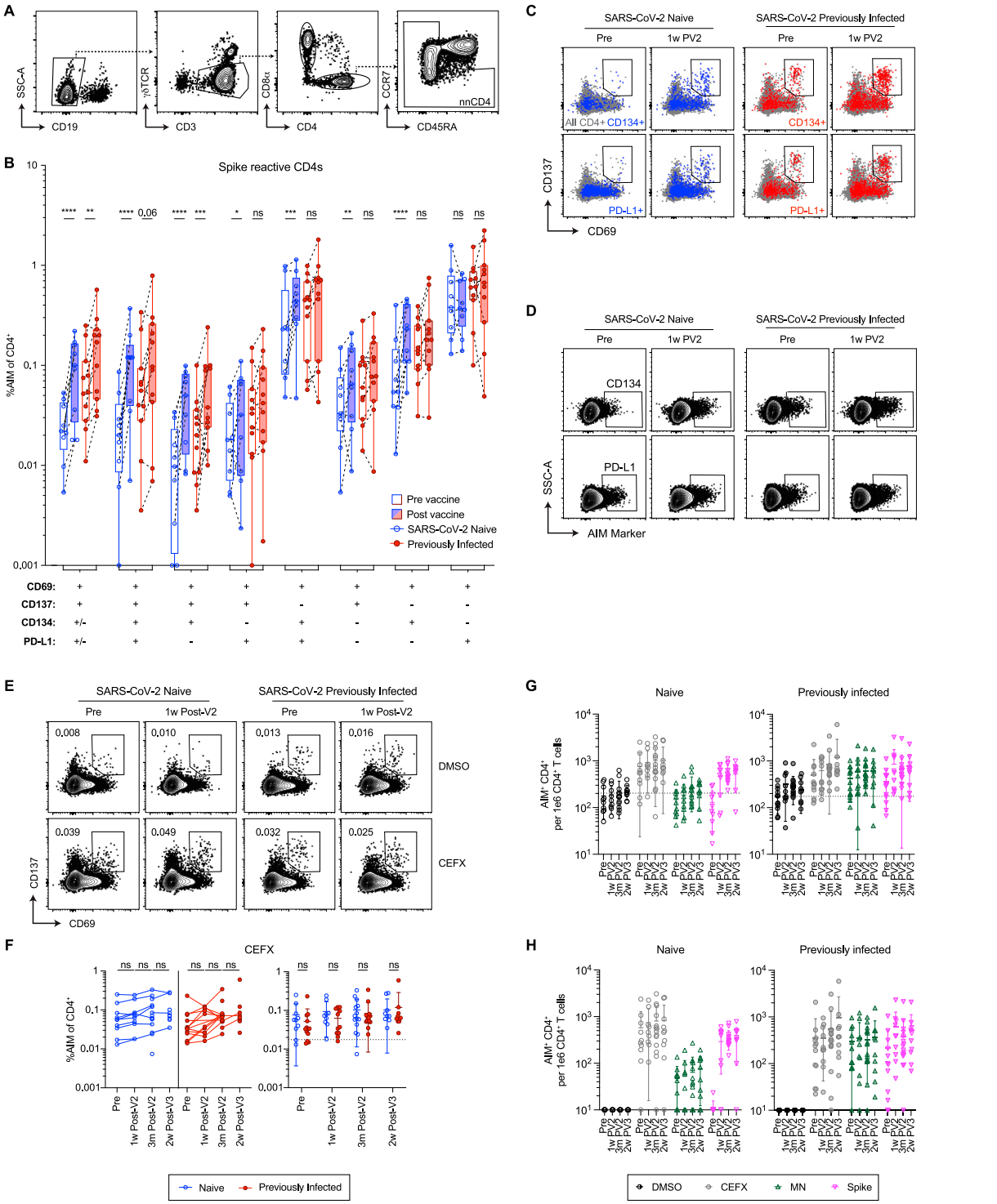

Figure S2. Determination of antigen-reactive activation markers in response to SARS-CoV-2 peptide stimulation and quantification of AIM CD4⁺ T cells, related to Figure 2

(A) Representative flow cytometry plots showing the gating schematic for non-naive (nn) CD4⁺ T cells (AIM CD4⁺).

(B) Boolean assessment of activation-associated markers on spike-reactive AIM CD4⁺ T cells from naive (blue) and previously infected (red) participants comparing pre-vaccine (Pre) and 1 week post two-dose mRNA vaccination (1w PV2). "+": marker was gated; "−": marker was excluded; "+/−": analysis was agnostic to indicated marker.

(legend continued on next page)

(C) Representative flow cytometry plots for AIM $CD4^+$ $CD69^+CD137^+$ T cells. Dot plot overlays show cells expressing additional activation-associated markers: CD134 (top) and PD-L1 (bottom).
(D) Representative flow cytometry plots for additional AIM markers CD134 and PD-L1.
(E and F) Representative flow cytometry plots and summary graphs for non-naive $CD69^+CD137^+$ T cells (AIM $CD4^+$) from SARS-CoV-2 naive (blue) and previously infected (red) individuals. Data in (F) are to a common antigen control peptide pool (CEFX) and represented both longitudinally (left) and by cross-group comparisons (right).
(G) Total AIM $CD4^+$ cell count per million $CD4^+$ T cells in each SARS-CoV-2 naive (left) and previously infected (right) donor.
(H) Background normalization of AIM $CD4^+$ T cell data from (G) was performed by subtracting DMSO cell counts from matched CEFX, M/N, and S samples. Significance was determined by Wilcoxon matched-paired signed rank test for longitudinal analyses and multiple unpaired Mann-Whitney test for group analyses: not significant (ns), *$p < 0.05$, **$p < 0.01$, ***$p < 0.001$, and ****$p < 0.0001$. Error bars represent mean and SD. Dashed lines indicate average donor background level. Pre-vaccination (Pre), 1 week post two-dose COVID-19 mRNA vaccination (1w PV2), 3 months post two-dose vaccination (3m PV2), 2 weeks post third vaccination dose (2w PV3).

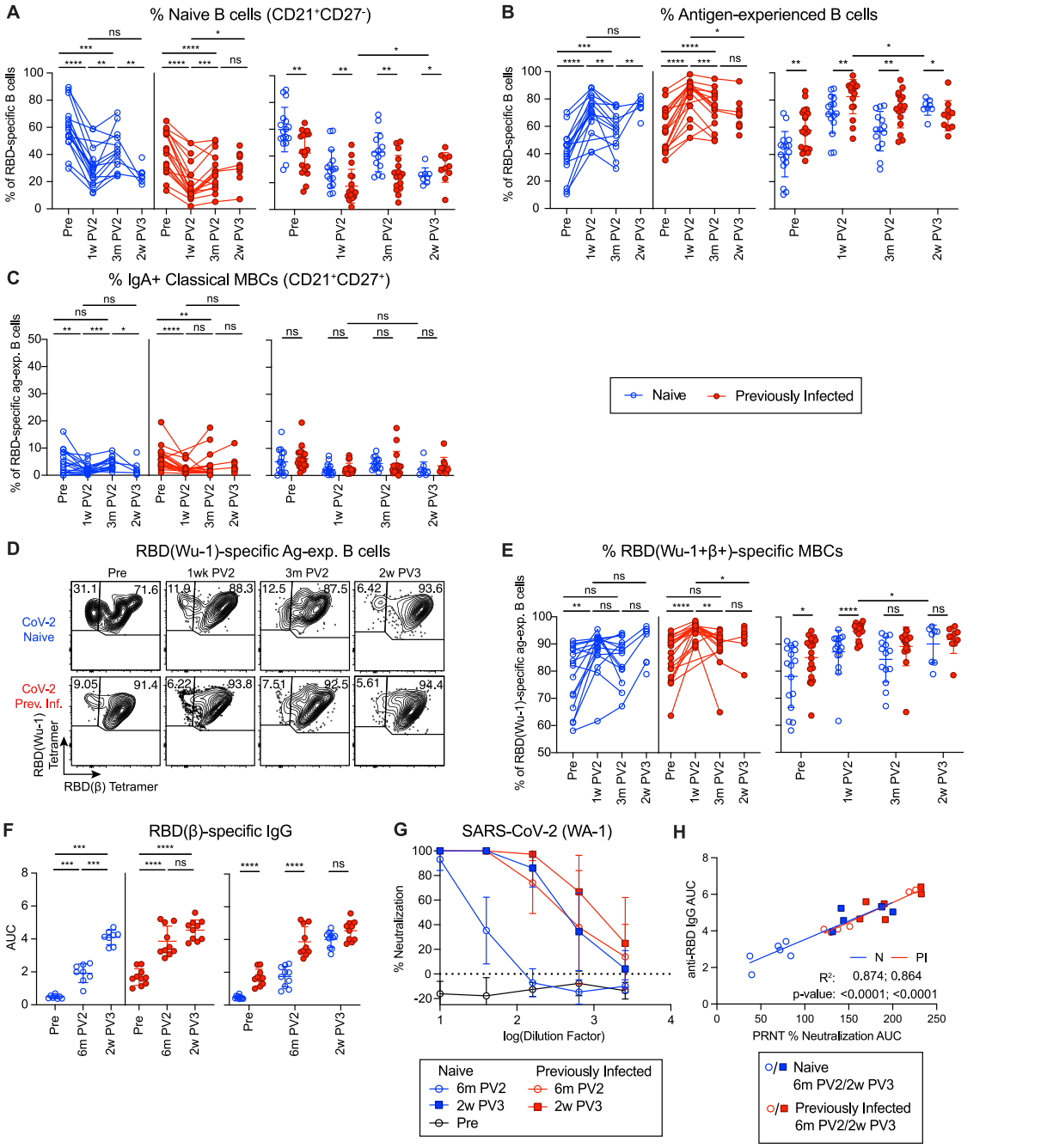

Figure S3. Vaccination induces enhanced variant binding and neutralizing breadth in RBD-specific MBCs and antibody in previously infected as compared with previously naive individuals, related to Figure 3

(A and B) (A) Percent naive B cells (CD21^{+}CD27^{-}) and (B) percent antigen-experienced (ag-exp.) B cells MBCs (CD21^{+}CD27^{+} and CD21^{-}CD27$^{+/-}$) of RBD-specific non-plasmablasts in N and PI PBMCs at the indicated time points.

(C) Percent IgG^{+} classical MBCs (CD21^{+}CD27^{+}) of RBD-specific ag-exp. B cells in N and PI PBMCs at the indicated time points.

(D) Representative gating on RBD(Wu-1)-specific antigen-experienced (ag-exp.) B cells for RBD(Wu-1) and RBD(β) tetramer binding to identify cross-variant specific RBD(Wu-1^{+}β^{+}) MBCs in N and PI PBMCs at the indicated time points.

(E) Percent RBD(Wu-1^{+}β^{+})-specific MBCs of RBD(Wu-1)-specific ag-exp. B cells in N and PI PBMCs at the indicated time points.

(F) ELISA area under the curve (AUC) for RBD(β)-specific IgG plasma antibody from N and PI individuals at indicated time points.

(G and H) (G) Percent neutralization of SARS-CoV-2(WA-1) virus by PRNT from N and PI individuals at the indicated time points and (H) correlation with RBD(Wu-1)-specific IgG AUC.

(legend continued on next page)

Data in (A–C), (E), and (F) are represented both longitudinally (left) and by cross-group comparisons (right). Statistics determined by two-tailed Mann-Whitney tests: not significant (ns), *$p < 0.05$, **$p < 0.005$, ***$p < 0.0005$, and ****$p < 0.0001$. Pre-vaccination (Pre), 1 week post two-dose COVID-19 mRNA vaccination (1w PV2), 3 months post two-dose vaccination (3m PV2), 2 weeks post third vaccination dose (2w PV3). Error bars represent mean and SD.

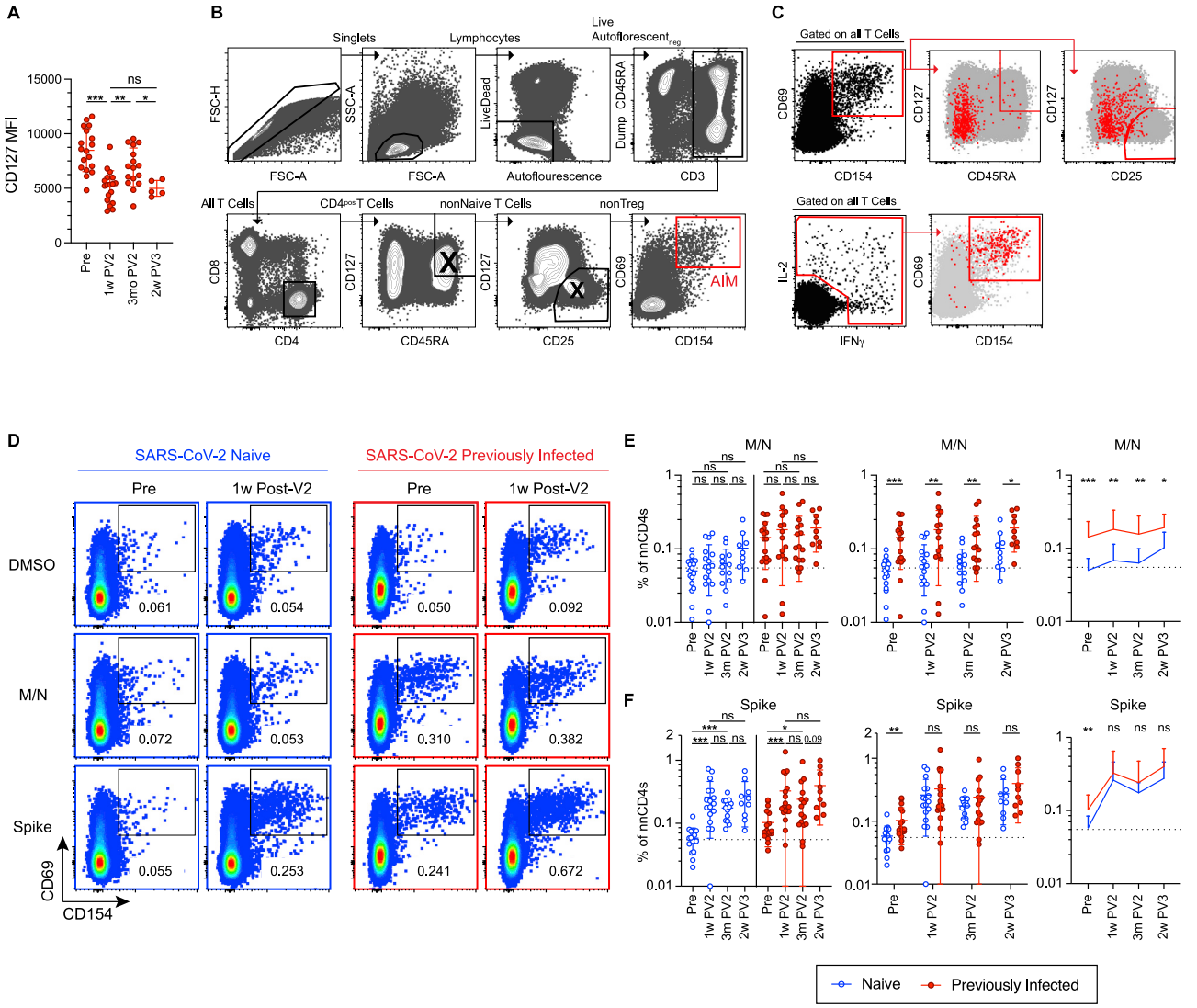

Figure S4. Gating strategy, validation, and assessment of total AIM CD4⁺CD69⁺CD154⁺ T cells from *ex vivo* cytokine release assay, related to Figure 4

(A) Mean fluorescent intensity (MFI) of CD127 on AIM CD4⁺ T cells in previously infected (red) participants.

(B) AIM gating strategy depicting removal of naive CD45RA⁺CD127⁺ T cells and CD25⁺CD127⁻ T regulatory cells.

(C) Validation of CD69⁺CD154⁺ AIM cells depicting absence from T regulatory and naive compartments (left) and inclusion of all cytokine-producing cells (right).

(D) Representative flow cytometry gating of non-naive (nn) AIM CD4⁺CD69⁺CD154⁺ T cells in DMSO-, M/N-, and S-stimulated memory T cells from SARS-CoV-2 naive (left, blue) and SARS-CoV-2 previously infected (right, red) participants before and 1 week after two doses of mRNA vaccine.

(E and F) Summary graphs of MN- (E) and S-specific (F) nnCD4⁺ T cells. Data in (E) and (F) are represented both longitudinally (left) and by cross-group comparisons (middle, right). Lines connecting data points indicate paired samples from the same donor. Significance was determined by Wilcoxon matched-paired signed rank test for longitudinal analyses and multiple unpaired Mann-Whitney test for group analyses: not significant (ns), *p < 0.05, **p < 0.01, ***p < 0.001. Error bars represent mean and SD. Dashed lines indicate average donor background level. Pre-vaccination (Pre), 1 week post two-dose COVID-19 mRNA vaccination (1w PV2), 3 months post two-dose vaccination (3m PV2), 2 weeks post third vaccination dose (2w PV3).

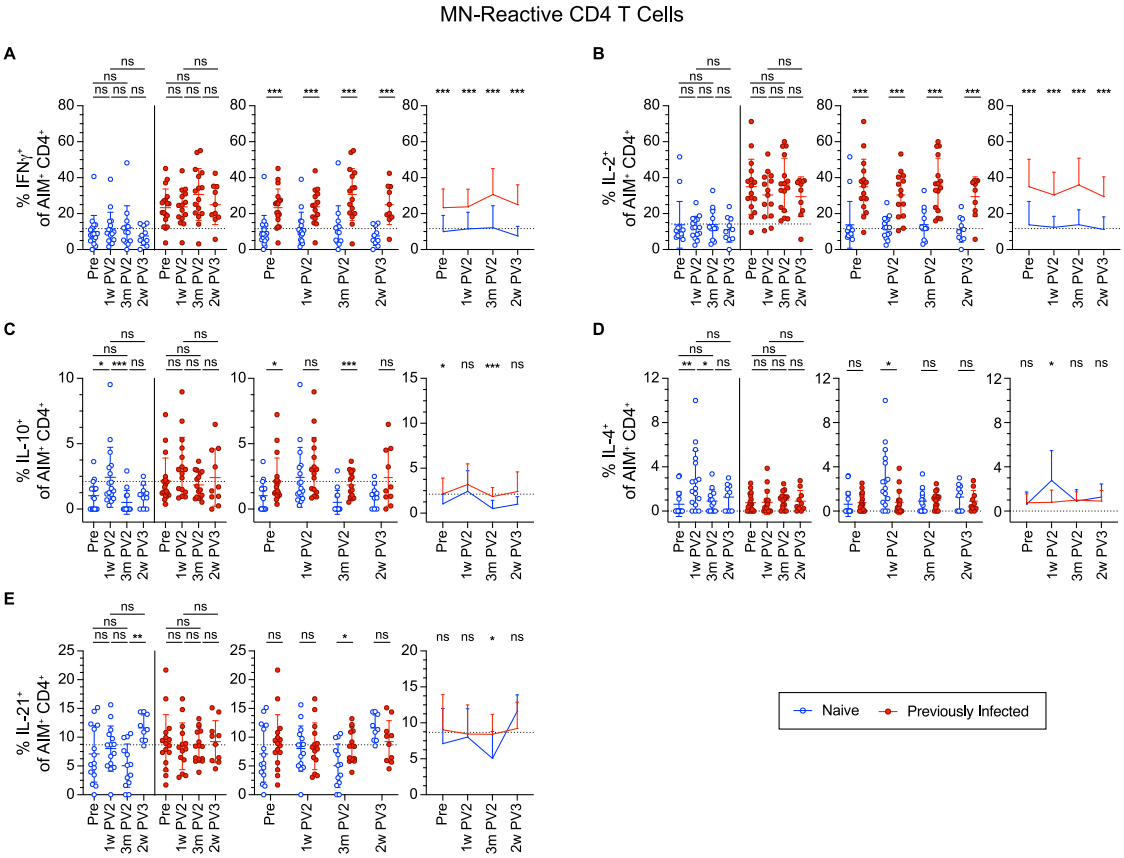

Figure S5. Cytokine production by M/N-specific AIM$^+$ CD4$^+$ T cells, related to Figure 4

(A–E) Summary graphs of the indicated cytokines for M/N-specific CD4$^+$CD69$^+$CD154$^+$ T cells (AIM$^+$CD4$^+$) in SARS-CoV-2 naive (blue) and previously infected (red) participants. Data are represented both longitudinally (left) and by cross-group comparisons (middle, right). Significance was determined by Wilcoxon matched-paired signed rank test for longitudinal analyses and multiple unpaired Mann-Whitney test for group analyses: not significant (ns), *p < 0.05, **p < 0.01, ***p < 0.001. Error bars represent mean and SD. Dashed lines indicate average donor background level. Pre-vaccination (Pre), 1 week post two-dose COVID-19 mRNA vaccination (1w PV2), 3 months post two-dose vaccination (3m PV2), 2 weeks post third vaccination dose (2w PV3).

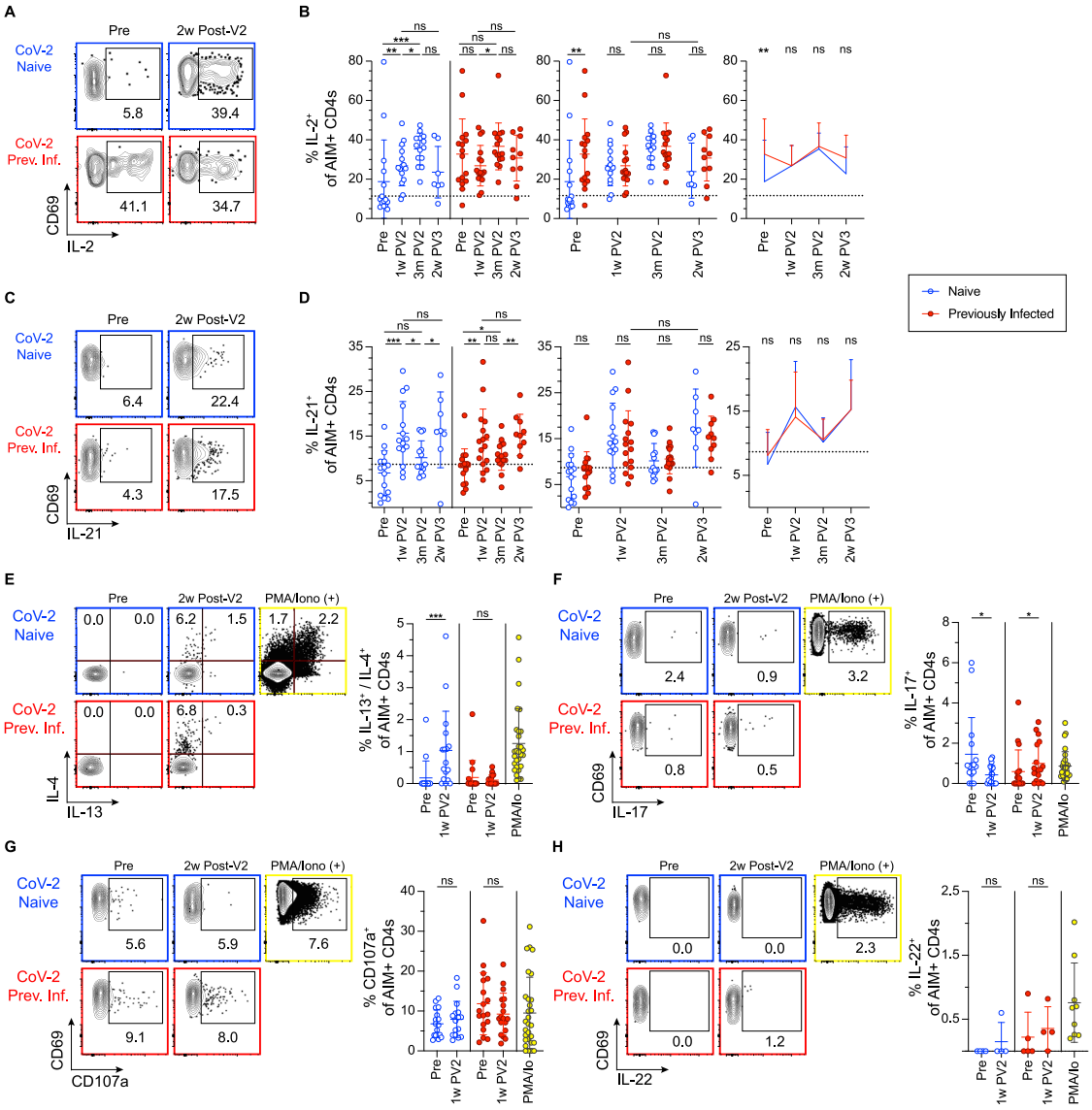

Figure S6. Supplemental cytokine production by S-specific AIM$^+$ CD4$^+$ T cells, related to Figure 4

(A–H) Representative flow cytometry plots and summary graphs for non-naive CD4$^+$CD69$^+$CD154$^+$ T cells (AIM$^+$ CD4s) for the indicated cytokines. Data in (B) and (D) are represented both longitudinally (left) and by cross-group comparisons (middle, right). Validation of cytokine staining for cases of very low cytokine producers indicated in (E) through (H) are provided using phorbol 12-myristate 13-acetate (PMA) and ionomycin positive control (yellow). Significance was determined by Wilcoxon matched-paired signed rank test for longitudinal analyses and multiple unpaired Mann-Whitney test for group analyses: not significant (ns), *p < 0.05, **p < 0.01, ***p < 0.001. Error bars represent mean and SD. Dashed lines indicate average donor background level. Pre-vaccination (Pre), 1 week post two-dose COVID-19 mRNA vaccination (1w PV2), 3 months post two-dose vaccination (3m PV2), 2 weeks post third vaccination dose (2w PV3).